Available online at http://jprm.sms.edu.pk/
Journal of Prime Research in Mathematics, 22(2) (2026), 50–81

Journal of Prime Research in Mathematics

Modeling the Impact of Susceptibility Heterogeneity in Diphtheria Outbreaks within a Vaccinated Population Using Fractional-Order Dynamics

Mohamad Tafrikan[a,b], Fatmawati[a,*], Windarto[a], Chinwendu E. Madubueze[c]

[a] *Department of Mathematics Faculty of Science and Technology, Airlangga University, Surabaya Indonesia.*
[b] *Department of Mathematics Faculty of Science and Technology, Walisongo State Islamic University, Semarang Indonesia.*
[c] *Department of Mathematics Faculty of Science and Technology, Joseph Sarwuan Tarka University, Makurdi Nigeria.*

Abstract

The purpose of this paper is to study a fractional mathematical model of diphtheria infection spread, considering the susceptibility heterogeneity subpopulation based on vaccination effects and an asymptomatic infected subpopulation. Memory effects and long-range interactions in all compartments are represented by a Caputo fractional derivative. The mathematical analysis of boundedness, positivity, and existence and uniqueness are discussed. We investigate local and global stability existence by applying **Matignon's theorem** and constructing an appropriate Lyapunov function. The local stability for disease-free equilibrium point is proved by applying the Routh–Hurwitz criterion. The global asymptotic stability of the disease-free equilibrium is examined by applying the approach proposed by Castillo-Chavez et al. And the predictor-corrector technique is used for the numerical simulation. We found that our approach perform better in terms stability region as compared to based-line models. We also present the comparasion result of root mean square error (RMSE) for varying fractional order alfa, and the $\alpha = 0.8$, give small RMSE, as to be considered by the goverment to reduce the Diphtheria outbreaks and to improve the vaccinated usage.

Keywords: Fractional-order model, Diphtheria, Stability analysis, Vaccination effects

1. Introduction and Preliminaries

An acute bacterial infection caused by Corynebacterium diphtheriae, diphtheria is a vaccine-preventable disease [56]. The disease spreads mainly via airborne respiratory droplets, direct contact with infected skin, or contaminated surfaces [35]. Although the case fatality rate reaches up to 50% in untreated, unvaccinated individuals, timely medical care can lower it to around 10% [12]. After an incubation period of 2–5 days,

*Corresponding author
Email addresses: tafrikan@walisongo.ac.id (Mohamad Tafrikan), fatmawati@fst.unair.ac.id (Fatmawati), windarto@fst.unair.ac.id (Windarto), madubueze.chinwendu@uam.edu.ng (Chinwendu E. Madubueze)

Received : 02 February 2026*; Accepted:* 22 May 2026*; Published Online:* 10 June 2026

symptoms can range from mild to severe, including respiratory distress, difficulty swallowing (dysphagia), and a persistent cough. Severe cases may lead to complications such as myocarditis, neuropathy, and renal failure [38]. A major complication in public health containment is the risk of transmission from asymptomatic carriers, which can persist for multiple weeks [7]. Therefore, the preventive strategy is built on vaccination, with a primary series of three doses in infancy and booster doses given during childhood and adolescence [46]. Hence, public health efforts that emphasize parents' understanding of the importance of complete immunization in reducing disease transmission need to be highlighted [30].

Indonesia recorded 7,886 diphtheria cases, with 339 deaths from 2012 to 2023. The outbreak peaked in 2018 with 1,386 infection cases, and the highest number of deaths, 46, occurred in 2022. Even though the national immunization program has been implemented, vaccination coverage remains low in some regions, particularly in Papua at 29.6% and Aceh at 49.6% [36]. In addition to vaccination, the Indonesian Ministry of Health also encourages strengthening the immune system through a healthy lifestyle, adequate nutrition, and proper sanitation as a preventive strategy. In this regard, a measured assessment to understand its impact on disease spread dynamics needs to be carried out. So one of the methods that can be used is mathematical modeling, defined as the process of formulating systems that exist in the real world and then converting them into equations to facilitate the understanding and study of complex phenomena [57, 42]. In epidemiology, mathematical models are crucial for simulating how diseases spread, understanding their transmission mechanisms, and predicting an outbreak. This provides a quantitative basis that can optimize public health strategies [10]. For example, the Susceptible-Infected-Recovered (SIR) model by Kermack and McKendrick [29] serves as a fundamental framework in infectious disease epidemiology. This model was later developed by Hethcote [23], who assumed a closed population. This approach has also been widely used in diphtheria models. Furthermore, research by [44], which shows that a combination of vaccination and quarantine is effective in controlling outbreaks, provided that vaccination coverage exceeds the 0.884 threshold and the minimum recovery rate is 0.04. Historical data from the Soviet Union in 1990 further supports the importance of vaccination, which can reduce infections by 11.31% [53], and analysis of epidemiological data from Thailand confirms that immunization is a key factor in reducing cases [1, 19, 25, 26, 52].

In addition to the implementation of vaccination, other studies also investigate the role of quarantine, such as research by [27, 45] which concluded that isolating individuals exposed to a disease can curb its spread, especially when combined with preventive strategies through natural immunity. In a similar manner, a study employing a mathematical model, which also contained a vaccinated population, revealed that a high level of vaccination can contribute to a marked slowing of disease spread [33]. Nevertheless, the continued persistence of diphtheria is a challenge that takes various forms. The continued persistence of disease spread due to reinfection, as evident through an SEIR model [50], indicates that a quarantine strategy alone will not suffice and will instead reach a level of endemism. Furthermore, contemporary SEIR models have advanced to incorporate distinct sub-populations. For example, the representation of extended recovery phases in Chikungunya [6] and the application of multi-compartment SEIQHRD frameworks to study COVID-19 dynamics at a regional level that illustrate the integer-order models manage high-dimensional complexity[28].

In recent decades, there has been an increasing trend in the research of models of a fractional order, because of their ability to account for memory properties, giving a more accurate description of biological processes [14, 15, 51] . These models have widely been applied in ecology, epidemiology, and the combined field of eco-epidemiology, in order to solve various problems [41, 51]. Application of fractional derivatives makes it possible to account for the memory and heritage properties, which are characteristic of various materials and processes [3, 37]. From the mathematical aspect, this memory effect is related to the presence of the nonlocal component in the system's solution, because in order to determine the present state, it is necessary to know the entire preceding history of the process [4, 9, 49]. A number of definitions have been introduced for designing fractional order derivatives, such as Riemann-Liouville, Caputo, Caputo-Fabrizio, and Atangana-Baleanu-Caputo derivatives [8, 11]. Therefore, Caputo derivatives can be considered as a preferred operator due to its dynamic properties, which are effective and outperform others with non-singular kernel definitions [51, 54]. In addition to model formulation, solving fractional differential

equations analytically is often difficult, especially for complex systems. Consequently, numerical methods play a crucial role in fractional-order modeling. A. Shakee et al. proposed the Polynomial Least Squares Method for fractional differential equations with Caputo derivatives, demonstrating high accuracy and fast convergence[48].

The model devised by [20] within the framework of the diphtheria epidemic considers the fractional derivative Caputo operator. The diphtheria model of Ghani et al. incorporates the Caputo fractional derivative; however, within their analysis, their work focused on establishing solution existence, uniqueness, and some numerical simulations due to limited literature on Caputo-based epidemiological models at that time. In this paper, we will establish our base on the Caputo operator, not only because of its richness in dynamics but also for an accurate calibration of the model for real-world diphtheria case data for better capturing the complex phenomena inherent in fractional-order systems. We focus on a comprehensive study of the fractional-order diphtheria model, that incorporates two critical features: susceptibility heterogeneity and asymptomatic infected population. Thus, our mathematical investigation involves the following: dynamical analysis regarding the understanding of the system's behavior, parameter estimation that fits the model to empirical data, sensitivity analysis to identify the most influential parameters, and numerical simulations for visualization of model outcomes, all in direct support of the core objectives pursued in this study, namely: rigorous stability analysis of the fractional-order diphtheria model and a detailed case study using diphtheria incidence data of Indonesia. Furthermore, we validate the fractional dynamical system (2.1) by fitting our fifth-order and fourth-order Runge-Kutta simulation results with real data using the least squares technique.

This paper is organized as follows. In Section 2, we present some basic definitions and necessary results that are useful for proving our main results (boundedness, non-negativity, existence, uniqueness, local stability, and global stability). This section also discusses the basic reproduction number derived using the next-generation matrix approach. Then, local stability is obtained through Matignon's Condition for the disease-free equilibrium point. The global stability of the disease-free equilibrium point is proven based on the method described in [10], and the global stability of the endemic equilibrium point is analyzed using a Goh–Volterra type Lyapunov function and LaSalle's invariance principle. In Section 4, we provide explanations of parameter estimation and sensitivity analysis. Next, the predictor-corrector technique is used for the numerical simulation approach. This numerical simulation is conducted to analyze the effect of fractional order on the model through simulations of various values of α, $\mathcal{R}_0$, η_1, η_2, w, and β. In addition, the validation of the fractional dynamic system (2.1) is also studied by matching the simulation results of the fifth-order and fourth-order Runge–Kutta methods with real data using the least squares technique.

2. Material and Methods

2.1. The Proposed Model

We present the definition of the Riemann–Liouville fractional integral as a basis for understanding the concept of fractional-order derivatives. In addition, the definition of the Caputo fractional derivative is also provided, which plays an important role as an operator in constructing the model in this study.

Definition 2.1. [17] Assume that $\alpha > 0$ and let $\mathcal{L}_1$ denote the Lebesgue space associated with the Taxicab norm. The Riemann–Liouville fractional integral of function X with order α is expressed as follows

$$\text{ORL } \mathcal{J}_t^{\alpha} X(t) = \frac{1}{\Gamma(n)} \int_0^t (t-s)^{\alpha-1} X(s)\, ds$$

for $t \in [0, T]$ and ORL $\mathcal{J}_t^{\alpha} \in \mathcal{L}_1([0, T])$

Definition 2.2. [17] For $\alpha > 0$, the Caputo fractional derivative of order α of a function $f \in C^n$ is defined as

$$D^{\alpha} f(t) = \frac{1}{\Gamma(n-\alpha)} \int_0^t \frac{f^{(n)}(s)}{(t-s)^{1+\alpha-n}}\, ds,$$

where Γ is the Gamma function and $n = \lceil \alpha \rceil$. In particular, if $0 < \alpha \leq 1$, then the expression for $D^{\alpha} f(t)$ becomes

$$D^{\alpha} f(t) = \frac{1}{\Gamma(1-\alpha)} \int_0^t \frac{f'(s)}{(t-s)^{\alpha}}\, ds.$$

Next this section, we present some lemmas, theorems, and corollary which are useful to prove the main results of our paper. We first give the comparison theorem which is useful to establish the boundedness.

Theorem 2.3. *[32, 31] Let $v(t) \in C\big([0,+\infty)\big)$, $\alpha \in (0,1]$, $\Phi, \Psi \in \mathbb{R}$, and $\Phi \neq 0$. If $v(t)$ satisfies*

$$D_*^{\alpha} v(t) \leq -\Phi v(t) + \Psi, \qquad v(0) = v_0 \in \mathbb{R},$$

then

$$v(t) \leq \left(v_0 - \frac{\Psi}{\Phi}\right) \mathcal{M}_{\alpha}(-\Phi t^{\alpha}) + \frac{\Psi}{\Phi},$$

where $\mathcal{M}_{\alpha}(k)$ is said to be the Mittag-Leffler function of one parameter and is defined by

$$\mathcal{M}_{\alpha}(k) = \sum_{j=0}^{\infty} \frac{k^j}{\Gamma(\alpha j + 1)}.$$

For the special, if $\alpha = 1$ then the equation above becomes the exponential function which has an important role in the classical calculus

$$e^k = \mathcal{M}_1(k) = \sum_{j=0}^{\infty} \frac{k^j}{\Gamma(j+1)}.$$

In [47], the correlations between the Mittag-Leffler and Wright functions are studied. The further lemma and corollary are presented to show the non-negativity of the solution in the system (1).

Lemma 2.4. *[40] Let $\big(v, D_*^{\alpha} v\big)(t) \in C\big([0,\zeta]\big)$ and $0 < \alpha \leq 1$. Then, one has*

$$v(t) = v(0) + \frac{1}{\Gamma(\alpha)}\, D_*^{\alpha} v(\xi)\, t^{\alpha},$$

where $\xi \in [0, y]$, for all $y \in [0, \xi)$.

Corollary 2.5. *[40] Let $\big(v, D_*^{\alpha} v\big)(t) \in C[0,\zeta]$ and $0 < \alpha \leq 1$. The function $v(t)$ is increasing for all $t \in (0,\zeta)$ if $D_*^{\alpha} v(t) \geq 0$, and it is decreased for all $t \in (0,\zeta)$ if $D_*^{\alpha} v(t) \leq 0$.*

Lemma 2.6. *[55] We consider $v(t) \in C(\mathbb{R}_+)$ and for any $0 < \alpha \leq 1$ the fractional system of order α exist. Then, one has*

$$D_*^{\alpha} \left[v(t) - v^* - v^* \ln \frac{v(t)}{v^*} \right] \leq \left(1 - \frac{v^*}{v(t)}\right) D_*^{\alpha} v(t),$$

$v^* \in \mathbb{R}_+$, for any $t > 0$.

Lemma 2.7. *[24] Suppose Ω is a set that is bounded and closed and every solution of*

$$D^{\alpha} v(t) = f\big(v(t)\big)$$

start from and remain in Ω for all time. If there exists a continuous function $V(v) : \Omega \to \mathbb{R}$ satisfying

$$D^{\alpha} V(v)|_{D^{\alpha} v(t) = f(v(t))} \leq 0,$$

where $\mathcal{K}$ is the largest set of variants of $E := \Big\{ v \;\Big|\; D^{\alpha} V(t)|_{D^{\alpha} v(t) = f(v(t))} = 0 \Big\}$. Then, for each solution $v(t)$ starting from Ω approaches to $\mathcal{K}$ as $t \to \infty$.

Observe that the Lyapunov function in Lemma 3 below can be expressed as $V(v)$. It is important to establish a Lyapunov function to satisfy Lemma 3. Furthermore, the negativity of a Lyapunov function tends to be established through Lemma 2.

This study is a development of the $SEIQR$ model [20] with the addition of a more detailed compartmental structure in the context of the Caputo derivative. Building on this, we propose a fractional-order diphtheria transmission model that considers vaccination and quarantine interventions. This model describes the dynamics of diphtheria transmission in more detail by dividing infected individuals into two categories: asymptomatic and symptomatic. In addition, the model distinguishes susceptible individuals based on their vaccination status, namely vaccinated and unvaccinated.

In the model (2.1), the exposed subpopulation (E) can change its status to infected (I) when symptoms appear, at a rate of $w\beta E$, where w is the proportion of infected individuals who are symptomatic and β is the infection rate. Meanwhile, the infected subpopulation without symptoms belongs to the asymptomatic infected subpopulation (A). The exposed subpopulation becomes subpopulation A at a rate of $(1-w)\beta E$. In addition, it is assumed that newborns can enter the S_2 group (vaccinated) only after reaching a minimum age of two months.

The flow of infection between model compartments is visualized in Figure 1 and the detailed definition of each parameter and its corresponding mathematical notation is systematically presented in Table 1.

Table 1: Definition of parameter

Parameter	Description
g	Proportion of the population that is vaccinated (vaccination coverage)
w	Proportion of symptomatic infected individuals
μ	Population birth rate (recruitment rate of susceptible individuals)
δ	Natural mortality rate (applies to all population compartments)
η_1	Effective contact rate between unvaccinated susceptible individuals (S_1) and infected individuals (I)
η_2	Effective contact rate between vaccinated susceptible individuals (S_2) and infected individuals (I)
β	**Infection rate from exposed** (E) to infected (I) state (inverse of incubation period)
γ	Rate of symptomatic infected individuals who are quarantined
ε	Recovery rate of infected individuals
θ	Mortality due to diphtheria
ρ	Rate of asymptomatic infected individuals who are quarantined

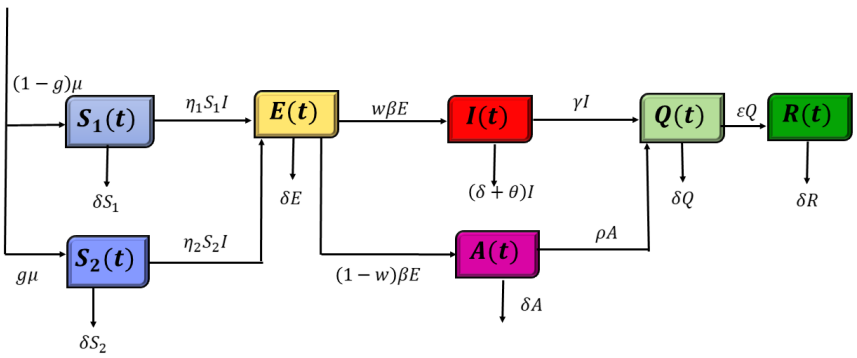

Figure 1: The compartmental structure of SEIAQR model

Our proposed model is expressed by system (2.1) using the Caputo derivative of order $\alpha \in (0,1]$, which is formulated as follows:

$$\begin{cases} D^\alpha S_1(t) = (1-g)\mu - (\delta + \eta_1 I)S_1, \\ D^\alpha S_2(t) = g\mu - (\delta + \eta_2 I)S_2, \\ D^\alpha E(t) = (\eta_1 S_1 + \eta_2 S_2)I - (\beta + \delta)E, \\ D^\alpha I(t) = w\beta E - (\gamma + \delta + \theta)I, \\ D^\alpha A(t) = (1-w)\beta E - (\rho + \delta)A, \\ D^\alpha Q(t) = \rho A + \gamma I - (\delta + \varepsilon)Q, \\ D^\alpha R(t) = \varepsilon Q - \delta R. \end{cases} \tag{2.1}$$

with initial values
$S_1(t_0) = S_1(0), S_2(t_0) = S_2(0), E(t_0) = E(0), I(t_0) = I(0), A(t_0) = A(0), Q(t_0) = Q(0), R(t_0) = R(0)$.

2.2. Boundedness and Non-Negativity

The developed model describes the transmission mechanism among subpopulations in the dynamics of diphtheria spread. Each subpopulation is represented by dependent variables such as S_1, S_2, E, I, A, Q, and R. Therefore, the model must have a unique solution to produce time-dependent dynamics of subpopulation sizes. Moreover, the obtained solution must be nonnegative, since subpopulation sizes cannot take negative values. On the other hand, resource limitations related to population size, such as food availability, healthcare services, and environmental conditions must also be considered. This implies that every solution produced must be bounded.

Thus, this section examines the existence, uniqueness, nonnegativity, and boundedness of the solutions of model (2.1) to ensure that the proposed model is valid in representing the real phenomenon of diphtheria transmission.

Theorem 2.8. *Given the initial conditions* $\{(S_1, S_2, E, I, A, Q, R) \geq 0\} \in \Omega$, *the solutions of system* (2.1) *are bounded in the biologically feasible region*

$$\Omega = \left\{ (S_1, S_2, E, I, A, Q, R) \in \mathbb{R}_+^7 : N(t) \leq \frac{\mu}{\delta} \right\}.$$

Proof. Let $N(t)$ be the total population of system (2.1), defined as $N(t) = S_1(t) + S_2(t) + E(t) + I(t) + A(t) + Q(t) + R(t)$. Next, by using the fractional derivative D^α, we obtain

$$\begin{aligned} D^\alpha N(t) &= D^\alpha S_1(t) + D^\alpha S_2(t) + D^\alpha E(t) + D^\alpha I(t) + D^\alpha A(t) + D^\alpha Q(t) + D^\alpha R(t) \\ &= \mu - \delta\left(S_1 + S_2 + E + I + A + Q + R\right) - \theta I \\ &= \mu - \delta N(t) - \theta I \\ &\leq \mu - \delta N(t). \end{aligned}$$

which implies that $D^\alpha N(t) + \delta N(t) \leq \mu$.

Based on the standard comparison theorem for fractional derivatives of order α (see [32, 31]), $D^\alpha N(t) \leq \mu - \delta N(t)$ leads to

$$N(t) \leq \left(N_0 - \frac{\mu}{\delta}\right) \mathcal{M}_\alpha(-\delta t^\alpha) + \frac{\mu}{\delta},$$

where $\mathcal{M}_\alpha$ is the Mittag-Leffler function. Moreover, Lemma 5 and Corollary 6 are applied in [13] to get $\mathcal{M}_\alpha(-\delta t^\alpha) \to 0$ as $t \to \infty$. As a result, obtained

$$\limsup_{t\to\infty} N(t) \leq \frac{\mu}{\delta}.$$

□

Theorem 2.9. *Given the initial values* $\{(S_1(0), S_2(0), E(0), I(0), A(0), R(0), Q(0)) \geq 0\} \in \varphi$ *of dynamical system* (2.1)*, the solution set* $\{S_1(t), S_2(t), E(t), I(t), A(t), R(t), Q(t)\}$ *of the system is non-negative for all* $t > 0$.

Proof. Consider $(2.1)_1$, one can derive

$$\begin{aligned} D^{\alpha} S_1(t) &= (1-g)\mu - (\delta + \eta_1 I) S_1 \\ &\geq -(\delta + \eta_1 I) S_1 \geq -\left(\delta + \frac{\eta_1 \mu}{\delta}\right) S_1, \end{aligned}$$

which means that

$$D^{\alpha} S_1(t) + \left(\delta + \frac{\eta_1 \mu}{\delta}\right) S_1 \geq 0.$$

Using the standard comparison theorem [32, 31], gives

$$S_1(t) \geq \left[(S_1(0) - 0)\, \mathcal{M}_{\alpha} \left\{ -\left(\delta + \frac{\eta_1 \mu}{\delta}\right) t^{\alpha} \right\} + 0 \right].$$

Since $\mathcal{M}_{\alpha} \left\{ -\left(\delta + \frac{\eta_1 \mu}{\delta}\right) t^{\alpha} \right\} \approx 0 \quad$ as $t \to \infty$, it can be concluded that $S_1(t) \geq 0$.
In addition, we can use a similar method to $(2.1)_2$, and one has

$$\begin{aligned} D^{\alpha} S_2(t) &= g\mu - (\delta + \eta_2 I) S_2 \\ &\geq -\left(\delta + \frac{\eta_2 \mu}{\delta}\right) S_2, \end{aligned}$$

which gives

$$D^{\alpha} S_2(t) + \left(\delta + \frac{\eta_2 \mu}{\delta}\right) S_2 \geq 0.$$

Because we have $S_2(t) \geq \left[(S_2(0) - 0)\, \mathcal{M}_{\alpha} \left\{ -\left(\delta + \frac{\eta_2 \mu}{\delta}\right) t^{\alpha} \right\} \right]$ and $\mathcal{M}_{\alpha} \left\{ -\left(\delta + \frac{\eta_2 \mu}{\delta}\right) t^{\alpha} \right\} \approx 0$ as $(t \to \infty)$ then the positivity of $S_2(t) \geq 0$ is achieved. Consequently, we have the same results for $(2.1)_3$, $(2.1)_4$, $(2.1)_5$, $(2.1)_6$ and $(2.1)_7$, by having $E(t) \geq (E(0) - 0)\, \mathcal{M}_{\alpha} \left\{ -(\beta + \delta) t^{\alpha} \right\}, I(t) \geq (I(0) - 0)\, \mathcal{M}_{\alpha} \left\{ -(\gamma + \delta + \theta) t^{\alpha} \right\}$, $A(t) \geq (A(0) - 0)\, \mathcal{M}_{\alpha} \left\{ -(\rho + \delta) t^{\alpha} \right\}, Q(t) \geq (Q(0) - 0)\, \mathcal{M}_{\alpha} \left\{ -(\delta + \varepsilon) t^{\alpha} \right\}, R(t) \geq (R(0) - 0)\, \mathcal{M}_{\alpha} \left\{ -\delta t^{\alpha} \right\}$, and $\mathcal{M}_{\alpha} \left\{ -(\beta + \delta) t^{\alpha} \right\} \approx 0, \mathcal{M}_{\alpha} \left\{ -(\gamma + \delta + \theta) t^{\alpha} \right\} \approx 0, \mathcal{M}_{\alpha} \left\{ -(\rho + \delta) t^{\alpha} \right\} \approx 0, \mathcal{M}_{\alpha} \left\{ -(\delta + \varepsilon) t^{\alpha} \right\} \approx 0$, $\mathcal{M}_{\alpha} \left\{ -\delta t^{\alpha} \right\} \approx 0$ as $t \to \infty$. Then, we can conclude that $E(t) \geq 0,\ I(t) \geq 0,\ A(t) \geq 0,\ Q(t) \geq 0,\ R(t) \geq 0$. □

2.3. Existence and Uniqueness

This section provides the **existence and uniqueness** of the fractional dynamical system (2.1) through the following maximality condition. Basically, the existence and uniqueness are the way to show the essence of first-order fractional dynamical system so that the given initial conditions can be satisfied.

Lemma 2.10. *Consider the constants* ℓ_k *and* $\bar{\ell}_k$*, such that*

$$|F_k(f_k, t) - F_k(f_k^*, t)|^2 \leq \ell_k |f_k - f_k^*|^2, \quad \forall (f, t) \in \left(\mathbb{R}^7 \times (0, T)\right), \tag{2.2}$$

and

$$|F_k(f_k, t)|^2 \leq \bar{\ell}_k \left(1 + |f_k|^2\right), \quad \forall (f, t) \in \left(\mathbb{R}^7 \times (0, T)\right). \tag{2.3}$$

Before we prove the existence and uniqueness of system (2.1) through (2.2) and (2.3), then as the first step, we assume that

$$\begin{aligned} F_1(t, S_1, S_2, E, I, A, Q, R) &:= D^{\alpha} S_1(t) = (1-g)\mu - (\delta + \eta_1 I) S_1, \\ F_2(t, S_1, S_2, E, I, A, Q, R) &:= D^{\alpha} S_2(t) = g\mu - (\delta + \eta_2 I) S_2, \\ F_3(t, S_1, S_2, E, I, A, Q, R) &:= D^{\alpha} E(t) = (\eta_1 S_1 + \eta_2 S_2) I - (\beta + \delta) E, \\ F_4(t, S_1, S_2, E, I, Q, R) &:= D^{\alpha} I(t) = w\beta E - (\gamma + \delta + \theta) I, \end{aligned}$$

$$
\begin{aligned}
F_5(t,S_1,S_2,E,I,A,Q,R) &:= D^{\alpha}A(t) = (1-w)\beta E - (\rho+\delta)A,\\
F_6(t,S_1,S_2,E,I,A,Q,R) &:= D^{\alpha}Q(t) = \rho A + \gamma I - (\delta+\varepsilon)Q,\\
F_7(t,S_1,S_2,E,I,A,Q,R) &:= D^{\alpha}R(t) = \varepsilon Q - \delta R,\\
(f_1,f_2,f_3,f_4,f_5,f_6,f_7) &:= (S_1,S_2,E,I,A,Q,R),\\
(f_1^*,f_2^*,f_3^*,f_4^*,f_5^*,f_6^*,f_7^*) &:= (S_1^*,S_2^*,E^*,I^*,A^*,Q^*,R^*).
\end{aligned} \tag{2.4}
$$

then, we first establish the following inequality

$$
|F_1(S_1,t) - F_1(S_1^*,t)|^2 \le \ell_1 |S_1 - S_1^*|^2 . \tag{2.5}
$$

It follows from (2.4), one has

$$
\begin{aligned}
|F_1(S_1,t) - F_1(S_1^*,t)|^2 &= |(1-g)\mu - (\delta+\eta_1 I)S_1 - (1-g)\mu + (\delta+\eta_1 I)S_1^*|^2 ,\\
&\le |(\delta+\eta_1 I)(S_1 - S_1^*)|^2 ,\\
&\le |\delta+\eta_1 I|^2 |S_1 - S_1^*|^2 ,\\
&\le (\delta + |\eta_1 I|)^2 |S_1 - S_1^*|^2 ,\\
&\le 2\left(\delta^2 + \eta_1^2 |I|^2\right)|S_1 - S_1^*|^2 ,\\
&\le 2\left(\delta^2 + \eta_1^2 \sup_{0\le t\le\kappa}|I|^2\right)|S_1 - S_1^*|^2 ,\\
&\le \ell_1 |S_1 - S_1^*|^2 ,
\end{aligned} \tag{2.6}
$$

where $\ell_1 = 2\left(\delta^2 + \eta_1^2 \sup\limits_{0\le t\le\kappa}|I|^2\right)$. In the same way, we obtain

$$
\begin{aligned}
&|F_2(S_2,t) - F_2(S_2^*,t)|^2 \le \ell_2 |S_2 - S_2^*|^2, \ell_2 = 2\left(\delta^2 + \eta_2^2 \sup_{0\le t\le\kappa}|I|^2\right),\\
&|F_3(E,t) - F_3(E^*,t)|^2 \le \ell_3 |E - E^*|^2, \ell_3 = 2(\beta^2+\delta^2),\\
&|F_4(I,t) - F_4(I^*,t)|^2 \le \ell_4 |I - I^*|^2, \ell_4 = 2(\gamma^2+\delta^2+\theta^2),\\
&|F_5(A,t) - F_5(A^*,t)|^2 \le \ell_5 |A - A^*|^2, \ell_5 = 2(\rho^2+\delta^2),\\
&|F_6(Q,t) - F_6(Q^*,t)|^2 \le \ell_6 |Q - Q^*|^2, \ell_6 = 2(\delta^2+\varepsilon^2),\\
&|F_7(R,t) - F_7(R^*,t)|^2 \le \ell_7 |R - R^*|^2, \ell_7 = \delta^2.
\end{aligned}
$$

Based on the above calculations, we can conclude that the first inequality (2.2) in Lemma 1 is satisfied. We continue to prove the second inequality (2.3) that the following inequality is satisfied

$$
|F_k(f_k,t)|^2 \le \bar{\ell}_k \left(1 + |f_k|^2\right). \tag{2.7}
$$

Firstly, we have

$$
\begin{aligned}
|F_1(S_1,t)|^2 &= |(1-g)\mu - (\delta+\eta_1 I)S_1|^2 ,\\
&\le (|(1-g)\mu| + |(\delta+\eta_1 I)S_1|)^2 ,\\
&\le 2\left((1-g)^2\mu^2 + \left(\delta^2 + \eta_1^2 \sup_{0\le t\le\kappa}|I(t)|^2\right)|S_1|^2\right),\\
&= 2((1-g)^2\mu^2 + 2\left(\delta^2 + \eta_1^2\|I\|_\infty^2\right)|S_1|^2),\\
&= 2(1-g)^2\mu^2 + 4\left(\delta^2 + \eta_1^2\|I\|_\infty^2\right)|S_1|^2,\\
&\le \bar{\ell}_1\left(1 + |S_1|^2\right),
\end{aligned} \tag{2.8}
$$

which gives $\frac{2(\delta^2+\eta_1^2\|I\|_\infty^2)}{(1-g)^2\mu^2} < 1$, where $\bar{\ell}_1 = \{2(1-g)\}^2\mu^2$. Applying the same strategy, obtained

$$\begin{aligned}
|F_2(S_2,t)|^2 &= |g\mu - (\delta+\eta_2 I)S_2|^2, \\
&\leq (|g\mu| + |(\delta+\eta_2 I)S_2|)^2, \\
&\leq 2\left(g^2\mu^2 + 2\left(\delta^2 + \eta_2^2 \sup_{0\leq t\leq\kappa}|I|^2\right)|S_2|^2\right), \\
&= 2(g^2\mu^2 + 2(\delta^2+\eta_2^2\|I\|_\infty^2)|S_2^2|), \\
&= 2g^2\mu^2 + 4(\delta^2+\eta_2^2\|I\|_\infty^2)|S_2|^2, \\
&\leq \bar{\ell}_2\left(1+|S_2|^2\right),
\end{aligned} \tag{2.9}$$

which gives $\frac{2(\delta^2+\eta_1^2\|I\|_\infty^2)}{g^2\mu^2} < 1$, where $\bar{\ell}_2 = 2g^2\mu^2$.

$$\begin{aligned}
|F_3(E,t)|^2 &= |(\eta_1 S_1 + \eta_2 S_2)I - (\beta+\delta)E|^2, \\
&\leq (|(\eta_1 S_1 + \eta_2 S_2)I| + |(\beta+\delta)E|)^2, \\
&\leq 2\Big((\eta_1^2 \sup_{0\leq t\leq\kappa}|S_1|^2 + \eta_2^2 \sup_{0\leq t\leq\kappa}|S_2|^2) \sup_{0\leq t\leq\kappa}|I|^2, \\
&\qquad + (\beta+\delta)^2|E|^2\Big), \\
&= 2\big((\eta_1^2\|S_1\|_\infty^2 + \eta_2^2\|S_2\|_\infty^2)\|I\|_\infty^2 + (\beta+\delta)^2|E|^2\big), \\
&= 2(\eta_1^2\|S_1\|_\infty^2 + \eta_2^2\|S_2\|_\infty^2)\|I\|_\infty^2 + 2(\beta+\delta)^2|E|^2, \\
&\leq \bar{\ell}_3(1+|E|^2),
\end{aligned} \tag{2.10}$$

which gives $\frac{(\beta+\delta)^2}{(\eta_1^2\|S_1\|_\infty^2+\eta_2^2\|S_2\|_\infty^2)\|I\|_\infty^2} < 1$, where $\bar{\ell}_3 = 2(\eta_1^2\|S_1\|_\infty^2 + \eta_2^2\|S_2\|_\infty^2)\|I\|_\infty^2$.

$$\begin{aligned}
|F_4(I,t)|^2 &= |w\beta E - (\gamma+\delta+\theta)I|^2, \\
&\leq (|w\beta E| + |(\gamma+\delta+\theta)I|)^2, \\
&\leq 2\big(w^2\beta^2 \sup_{0\leq t\leq\kappa}|E|^2 + (\gamma+\delta+\theta)^2|I|^2\big), \\
&= 2\big(w^2\beta^2\|E\|_\infty^2 + (\gamma+\delta+\theta)^2|I|^2\big), \\
&= 2w^2\beta^2\|E\|_\infty^2 + 2(\gamma+\delta+\theta)^2|I|^2, \\
&\leq \bar{\ell}_4(1+|I|^2),
\end{aligned} \tag{2.11}$$

which gives $\frac{(\gamma+\delta+\theta)^2}{w^2\beta^2\|E\|_\infty^2} < 1$, where $\bar{\ell}_4 = 2w^2\beta^2\|E\|_\infty^2$.

$$\begin{aligned}
|F_5(I,t)|^2 &= |(1-w)\beta E - (\rho+\delta)A|^2, \\
&\leq (|(1-w)\beta E| + |(\rho+\delta)A|)^2, \\
&\leq 2\big((1-w)^2\beta^2 \sup_{0\leq t\leq\kappa}|E|^2 + (\rho+\delta)^2|A|^2\big), \\
&= 2\big((1-w)^2\beta^2\|E\|_\infty^2 + (\rho+\delta)^2|A|^2\big), \\
&= 2(1-w)^2\beta^2\|E\|_\infty^2 + 2(\rho+\delta)^2|A|^2, \\
&\leq \bar{\ell}_5(1+|A|^2),
\end{aligned} \tag{2.12}$$

which gives $\frac{(\rho+\delta)^2}{(1-w)^2\beta^2\|E\|_\infty^2} < 1$, where $\bar{\ell}_5 = 2(1-w)^2\beta^2\|E\|_\infty^2$.

$$\begin{aligned} |F_6(Q,t)|^2 &= |\rho A + \gamma I - (\delta+\varepsilon)Q|^2 \\ &\leq (|\rho A| + |\gamma I| + |(\delta+\varepsilon)Q|)^2, \\ &\leq 2\big(\rho^2 \sup_{0\leq t\leq \kappa} |A|^2 + \gamma^2 \sup_{0\leq t\leq \kappa} |I|^2 + (\delta+\varepsilon)^2|Q|^2\big), \\ &= 2\big(\rho^2\|A\|_\infty^2 + \gamma^2\|I\|_\infty^2 + (\delta+\varepsilon)^2|Q|^2\big), \\ &= 2\rho^2\|A\|_\infty^2 + 2\gamma^2\|I\|_\infty^2 + 2(\delta+\varepsilon)^2|Q|^2, \\ &\leq \bar{\ell}_6(1+|Q|^2), \end{aligned} \tag{2.13}$$

which gives $\frac{(\delta+\varepsilon)^2}{\gamma^2\|I\|_\infty^2+\rho^2\|A\|_\infty^2} < 1$, where $\bar{\ell}_6 = 2(\gamma^2\|I\|_\infty^2 + \rho^2\|A\|_\infty^2)$.

$$\begin{aligned} |F_7(R,t)|^2 &= |\varepsilon Q - \delta R|^2 \\ &\leq (|\varepsilon Q| + |\delta R|)^2, \\ &\leq 2\big(\varepsilon^2 \sup_{0\leq t\leq \kappa} |Q|^2 + \delta^2|R|^2\big), \\ &= 2\big(\varepsilon^2\|Q\|_\infty^2 + \delta^2|R|^2\big), \\ &= 2\varepsilon^2\|Q\|_\infty^2 + 2\delta^2|R|^2, \\ &\leq \bar{\ell}_7(1+|R|^2), \end{aligned} \tag{2.14}$$

which gives $\frac{\delta^2}{\varepsilon^2\|Q\|_\infty^2} < 1$, where $\bar{\ell}_7 = 2\varepsilon^2\|Q\|_\infty^2$. Finally, the second inequality (2.3) can be established in the following maximality condition

$$\max\left\{\begin{array}{l} \frac{2(\delta^2+\eta^2\|I\|_\infty^2)}{(1-g)^2\mu^2}, \frac{2(\delta^2+\eta^2\|I\|_\infty^2)}{g^2\mu^2}, \frac{(\beta+\delta)^2}{\eta_1^2\|S_1\|_\infty^2+\eta_2^2\|S_2\|_\infty^2\|I\|_\infty^2}, \frac{(\gamma+\delta+\theta)^2}{w^2\beta^2\|E\|_\infty^2}, \\ \frac{(\gamma+\delta+\theta)^2}{(1-w)^2\beta^2\|E\|_\infty^2}, \frac{(\delta+\varepsilon)^2}{\gamma^2\|I\|_\infty^2+\rho^2\|A\|_\infty^2}, \frac{\delta^2}{\varepsilon^2\|Q\|_\infty^2} \end{array}\right\} < 1.$$

2.3.1. Equilibrium of Disease-Free Point

An equilibrium point describes a state where the population size in each group remains constant over time, or in other words, the rate of change is zero. Based on this concept, the diphtheria transmission model qualifies to achieve a Disease-Free Equilibrium (DFE), denoted as ε_0 . This condition occurs when there is no disease present in the population, meaning no individuals are infected ($I = A = 0$). In the system of model (2.1) the disease-free equilibrium point is expressed as follows:

$$\varepsilon_0 = (S_1^0, S_2^0, E^0, I^0, A^0, Q^0, R^0) = \left(\frac{(1-g)\mu}{\delta}, \frac{g\mu}{\delta}, 0, 0, 0, 0, 0\right). \tag{2.15}$$

2.3.2. Basic Reproduction Number

The basic reproduction number $\mathcal{R}_0$ represents the estimated number of people who contract an infection from a single case in a completely susceptible population. For $\mathcal{R}_0 < 1$, each infected individual transmits the disease to fewer than one person on average, causing the outbreak to gradually die out. Conversely, when $\mathcal{R}_0 > 1$, sustained transmission occurs because each infected individual spreads the disease to more than one person, allowing the pathogen to persist long-term and potentially become endemic.

Currently, there is no method available for fractional-order mathematical models in determining the basic reproduction number. Therefore, in accordance with the fractional model [2, 20], the calculation of $\mathcal{R}_0$ is independent of the fractional order α and performed by analyzing the dominant eigenvalue of the Next Generation Matrix [16]. Using a linear approximation near the disease-free equilibrium (ε_0), we obtain the following result:

$$J = \begin{bmatrix} 0 & \eta_1 S_1 + \eta_2 S_2 & 0 \\ 0 & 0 & 0 \\ 0 & 0 & 0 \end{bmatrix} - \begin{bmatrix} \delta+\beta & 0 & 0 \\ -w\beta & \gamma+\delta+\theta & 0 \\ -(1-w)\beta & 0 & \rho+\delta \end{bmatrix}, \tag{2.16}$$
$$J = F - V.$$

In this context, matrix F serves as the mathematical representation of the rate of new infections, while matrix V models the transition dynamics of subpopulations between epidemiological compartments. Based on this formulation, the basic reproduction number $\mathcal{R}_0$ is mathematically equivalent to the spectral radius (dominant eigenvalue) derived from the matrix operation $K = FV^{-1}$.

$$|\lambda I - K| = \begin{vmatrix} \lambda - \frac{w\beta(\eta_1(1-g)\mu+\eta_2 g\mu)}{\delta(\delta+\beta)(\gamma+\delta+\theta)} & -\frac{\eta_1(1-g)\mu+\eta_2 g\mu}{\delta(\gamma+\delta+\theta)} & 0 \\ 0 & \lambda & 0 \\ 0 & 0 & \lambda \end{vmatrix},$$

which gives $\lambda_1 = \frac{w\beta\mu\left(\eta_1(1-g)+\eta_2 g\right)}{\delta(\delta+\beta)(\gamma+\delta+\theta)}$ and $\lambda_2 = \lambda_3 = 0$. Thus, for model (2.1) the basic reproduction number can be expressed by the equation:

$$\mathcal{R}_0 = \frac{w\beta\mu\left(\eta_1(1-g)+\eta_2 g\right)}{\delta(\delta+\beta)(\gamma+\delta+\theta)}. \tag{2.17}$$

2.3.3. Local Stability of Disease-Free Equilibrium Point

The stability of equilibrium points is a critical aspect of disease modeling. By analyzing the sufficient conditions for equilibrium stability, we can evaluate the potential for the diphtheria epidemic to become endemic. This section examines the local stability of the equilibrium points by linearizing the model (2.1) around the equilibrium point, which has the Jacobian matrix

$$J = \begin{bmatrix} -(\delta+\eta_1 I) & 0 & 0 & -\eta_1 S_1 & 0 & 0 & 0 \\ 0 & -(\delta+\eta_2 I) & 0 & -\eta_2 S_2 & 0 & 0 & 0 \\ \eta_1 I & \eta_2 I & -(\delta+\beta) & (\eta_1 S_1+\eta_2 S_2) & 0 & 0 & 0 \\ 0 & 0 & w\beta & -(\gamma+\delta+\theta) & 0 & 0 & 0 \\ 0 & 0 & (1-w)\beta & 0 & -(\rho+\delta) & 0 & 0 \\ 0 & 0 & 0 & \gamma & \rho & -(\delta+\varepsilon) & 0 \\ 0 & 0 & 0 & 0 & 0 & \varepsilon & -\delta \end{bmatrix}. \tag{2.18}$$

To analyze the local stability of the equilibrium points, the Jacobian matrix of the system is evaluated at the corresponding equilibrium. According to the stability criterion for fractional-order systems of order αgiven by [34, 43], an equilibrium point is asymptotically stable if all eigenvalues λ_i of the Jacobian matrix satisfy the condition $|\arg(\lambda_i)| > \frac{\alpha\pi}{2}$. This criterion, known as the Matignon condition, is applied to the eigenvalues obtained from the Jacobian matrix at the disease-free and endemic equilibrium points to determine their stability.

Theorem 2.11. *The disease-free equilibrium point of the system of equations* (2.1) *is locally asymptotically stable if* $\mathcal{R}_0 < 1$*, and locally asymptotically unstable if* $\mathcal{R}_0 > 1$*.*

Proof. The Jacobian matrix of the dynamical system (2.1) at ε_0 is given as follows

$$J(\varepsilon_0) = \begin{bmatrix} -\delta & 0 & 0 & -\frac{\eta_1(1-g)\mu}{\delta} & 0 & 0 & 0 \\ 0 & -\delta & 0 & -\frac{\eta_2 g\mu}{\delta} & 0 & 0 & 0 \\ 0 & 0 & -(\delta+\beta) & \frac{(\eta_1(1-g)+\eta_2 g)\mu}{\delta} & 0 & 0 & 0 \\ 0 & 0 & w\beta & -(\gamma+\delta+\theta) & 0 & 0 & 0 \\ 0 & 0 & (1-w)\beta & 0 & -(\rho+\delta) & 0 & 0 \\ 0 & 0 & 0 & \gamma & \rho & -(\delta+\varepsilon) & 0 \\ 0 & 0 & 0 & 0 & 0 & \varepsilon & -\delta \end{bmatrix}. \tag{2.19}$$

the eigenvalues of (2.18) are obtained by the solution of characteristic equation $|\lambda I - J(\varepsilon_0)| = 0$, then we obtain

$$(\lambda+\delta)(\lambda+(\delta+\varepsilon))(\lambda+(\delta+\rho))(\lambda+\delta)(\lambda+\delta)M = 0, \tag{2.20}$$

with $M = (\lambda+(\gamma+\delta+\theta))(\lambda+(\delta+\beta)) - \frac{w\beta(\eta_1(1-g)+\eta_2 g)\mu}{\delta}$, we obtain the eigenvalues corresponding to characteristic Equation (2.19) are

$$\lambda_1 = \lambda_2 = \lambda_3 = -\delta, \quad \lambda_4 = -(\delta+\varepsilon), \quad \lambda_5 = -(\delta+\rho).$$

It is clear that $\delta, \varepsilon, \rho > 0$, then all of these eigenvalues have a negative real part. Hence, the eigenvalues satisfy $|\arg(\lambda_i)| = \pi > \frac{\alpha\pi}{2}$ for all $i = 1, 2, 3, 4, 5$, which is a stable region of equilibrium point. Other eigenvalues are obtained from the Equation (2.19) $M(\lambda) = 0$, which can be rewritten as

$$\lambda^2 + m_1\lambda + m_0 = 0,$$

where

$$m_1 = (\gamma+\delta+\theta)+(\delta+\beta), \quad m_0 = (\gamma+\delta+\theta)(\delta+\beta)(1-\mathcal{R}_0),$$

and

$$\mathcal{R}_0 = \frac{w\beta\mu\,(\eta_1(1-g)+\eta_2 g)}{\delta(\delta+\beta)(\gamma+\delta+\theta)}.$$

Based on the modified Routh–Hurwitz criterion for fractional systems [5], the equation $\lambda^2+m_1\lambda+m_0 = 0$ has roots with negative real parts if and only if $m_1 > 0$ and $m_0 > 0$. Since all parameters are positive, $m_1 > 0$ is always satisfied. Meanwhile, $m_0 > 0$ is satisfied if and only if $\mathcal{R}_0 < 1$. Thus, all eigenvalues λ_6, λ_7 satisfy $|\arg(\lambda_i)| = \pi > \frac{\alpha\pi}{2}$ for all $i = 6, 7$, if $\mathcal{R}_0 < 1$, which guarantees local asymptotic stability. Therefore, the disease-free equilibrium point (ε_0) is locally asymptotically stable if $\mathcal{R}_0 < 1$ and unstable if $\mathcal{R}_0 > 1$. □

2.3.4. Global Stability of Disease-Free Equilibrium Point

Global stability analysis of equilibrium points in epidemic models is crucial for predicting transmission patterns and evaluating the impact of control policies. The global asymptotic stability of the disease-free equilibrium is examined by applying the approach proposed by [10], which has been widely utilized in analyzing epidemic models to demonstrate convergence toward a disease-free state. According to this approach, the system is written as

$$\begin{aligned} D^\alpha X &= F(X, Z), \\ D^\alpha Z &= G(X, Z), \quad G(X, 0) = 0 \end{aligned} \tag{2.21}$$

where $X = (S_1, S_2, R)^T \in \mathbb{R}^3$ represents the number of uninfected classes, $Z = (E, I, A, Q)^T \in \mathbb{R}^4$ represents the number of infected classes, and $\varepsilon_0 = (X_0, 0)$ denotes the disease- free equilibrium of the system.

The disease-free equilibrium ε_0 is globally asymptotically stable if the following conditions are satisfied:

(H1) For $D^\alpha X = F(X, 0)$, the equilibrium point X_0 is globally asymptotically stable.

(H2) $\hat{G}(X,Z) = AZ - G(X,Z)$, $\hat{G}(X,Z) \geq 0$ for $(X,Z) \in \Omega$, where $A = D_Z G(X_0, 0)$ is the M-matrix whose off-diagonal elements are nonnegative.

The discussion regarding the global stability of ε_0 can be presented in the proof of the following theorem.

Theorem 2.12. *The disease-free equilibrium of system* (2.1) *is globally asymptotically stable when the disease-induced death rates are ignored* ($\theta = 0$) *and* $\mathcal{R}_0 < 1$. *Moreover, the equilibrium is given by*

$$\varepsilon_0 = (X_0, 0) = \left(\frac{(1-g)\mu}{\delta}, \frac{g\mu}{\delta}, 0, 0, 0, 0 \right).$$

Proof. From system (2.20) the following functions are obtained:

$$F(X,Z) = \begin{pmatrix} (1-g)\mu - (\delta + \eta_1 I)S_1 \\ g\mu - (\delta + \eta_2 I)S_2 \\ \varepsilon Q - \delta R \end{pmatrix},$$

$$G(X,Z) = \begin{pmatrix} (\eta_1 S_1 + \eta_2 S_2)I - (\beta + \delta)E \\ w\beta E - (\gamma + \delta + \theta)I \\ (1-w)\beta E - (\rho + \delta)A \\ \rho A + \gamma I - (\delta + \varepsilon)Q \end{pmatrix}.$$

Furthermore, we obtain

$$A = \begin{pmatrix} -(\beta+\delta) & \eta_1 S_{1_0} + \eta_2 S_{2_0} & 0 & 0 \\ w\beta & -(\gamma+\delta+\theta) & 0 & 0 \\ (1-w)\beta & 0 & -(\rho+\delta) & 0 \\ 0 & \gamma & \rho & -(\delta+\varepsilon) \end{pmatrix}, F(X,0) = \begin{pmatrix} (1-g)\mu - \delta S_1 \\ g\mu - \delta S_2 \\ -\delta R \end{pmatrix},$$

$$\hat{G}(X,Z) = \begin{pmatrix} (\eta_1 S_{1_0} + \eta_2 S_{2_0}) I \left(1 - \dfrac{\eta_1 S_1 + \eta_2 S_2}{\eta_1 S_{1_0} + \eta_2 S_{2_0}} \right) \\ 0 \\ 0 \\ 0 \end{pmatrix}.$$

By solving $D^\alpha X = F(X,0)$, we obtain

$$\begin{pmatrix} D^\alpha S_1(t) \\ D^\alpha S_2(t) \\ D^\alpha R(t) \end{pmatrix} = \begin{pmatrix} \dfrac{(1-g)\mu}{\delta} + \left(S_1(0) - \dfrac{(1-g)\mu}{\delta} \right) e^{-\delta t} \\ \dfrac{g\mu}{\delta} + \left(S_2(0) - \dfrac{g\mu}{\delta} \right) e^{-\delta t} \\ R(0) e^{-\delta t} \end{pmatrix}. \tag{2.22}$$

From Equation (2.21), by setting $Z = 0$, we have $\lim_{t\to\infty} S_1(t) = \dfrac{(1-g)\mu}{\delta}$, $\lim_{t\to\infty} S_2(t) = \dfrac{g\mu}{\delta}$, $\lim_{t\to\infty} R(t) = 0$. This indicates that the equilibrium point $X_0 = \left(\frac{(1-g)\mu}{\delta}, \frac{g\mu}{\delta}, 0 \right)$ is globally asymptotically stable, there by satisfying condition H_1. Next, it is clear that $\widehat{G_2}(X,Z) \geq 0, \widehat{G_3}(X,Z) \geq 0, \widehat{G_4}(X,Z) \geq 0, \text{and} S_1 \leq S_{1_0}$, $S_2 \leq S_{2_0}$. However, in order to have $\widehat{G_1}(X,Z) \geq 0$, some additional conditions are required. For example, we may assume that the total human population is at the equilibrium level ($N = N_0$) and this condition will be satisfied if the disease-induced death rate is ignored ($\theta = 0$). This ensures that $1 - \frac{\eta_1 S_1 + \eta_2 S_2}{\eta_1 S_{1_0} + \eta_2 S_{2_0}} \geq 0$. Hence, condition H_2 is satisfied. Since both conditions are fulfilled, the disease-free equilibrium is globally asymptotically stable if the disease-induced death rate is ignored. □

2.4. Endemic Equilibrium Point

This section examines the equilibrium condition where the disease persists in the population (the endemic equilibrium point ε_1 of model (2.1)), which occurs when the number of infected individuals (I^*) is non-zero. By substituting ε_1 into model (2.1), we obtain the following relationship:

$$\begin{aligned}\varepsilon_1 &= (S_1^*, S_2^*, E^*, I^*, A^*, Q^*, R^*) \\ &= \left(\frac{(1-g)\mu}{\delta+\eta_1 I^*}, \frac{g\mu}{\delta+\eta_2 I^*}, \frac{\mu I^* \left(\frac{\eta_1(1-g)}{\delta+\eta_1 I^*} + \frac{\eta_2 g}{\delta+\eta_2 I^*}\right)}{\beta+\delta}, I^*, \frac{(1-w)\beta\mu I^* \left(\frac{\eta_1(1-g)}{\delta+\eta_1 I^*} + \frac{\eta_2 g}{\delta+\eta_2 I^*}\right)}{(\rho+\delta)(\beta+\delta)}, \frac{\rho A^* + \gamma I^*}{\delta+\varepsilon}, \frac{\varepsilon Q^*}{\delta} \right)\end{aligned} \tag{2.23}$$

where I^* satisfies the characteristic equation:

$$\Lambda_1 I^{*2} + \Lambda_2 I^* + \Lambda_3 = 0 \tag{2.24}$$

with coeficient $\Lambda_1 = \eta_1\eta_2, \Lambda_2 = \delta\left((\eta_1+\eta_2) - \frac{\mathcal{R}_0\eta_1\eta_2}{\eta_1(1-g)+\eta_2 g}\right)$, and $\Lambda_3 = \delta^2(1-\mathcal{R}_0)$. For $\mathcal{R}_0 < 1$, the discriminant (D) of (2.24) is :

$$D = \left(\delta\left((\eta_1+\eta_2) - \frac{\mathcal{R}_0\eta_1\eta_2}{\eta_1(1-g)+\eta_2 g}\right)\right)^2 - 4\eta_1\eta_2\delta^2(1-\mathcal{R}_0).$$

Based on arithmetic-geometric inequality, we have $\eta_1+\eta_2 \geq \sqrt{\eta_1\eta_2}$, the discriminant value D will always be negative, we conclude that the Equation (2.24) has no solution for $\mathcal{R}_0 < 1$.

2.5. Endemic Global stability

In this subsection, we analyze the global asymptotic stability of the endemic equilibrium of system (2.1). For that purpose, the invariant set Ω_0 is first defined as follows.

Suppose

$$\Omega_0 = \{M \in \Omega : E = I = A = Q = 0\},$$

where $M = \left(D^\alpha S_1(t), D^\alpha S_2(t), D^\alpha E(t), D^\alpha I(t), D^\alpha A(t), D^\alpha Q(t), D^\alpha R(t)\right)$, and Ω_0 represents the stable manifold of the non-endemic equilibrium ε_0. The global stability of the endemic equilibrium is stated in the following theorem.

Theorem 2.13. *The endemic equilibrium ε^* in the special case is globally asymptotically stable in the interior of the region $\Omega \setminus \Omega_0$ if $\mathcal{R}_0 > 1$.*

Proof. Using a Goh-Volterra type Lyapunov function $\mathcal{L} : \Omega \setminus \Omega_0 \to \mathbb{R}$ defined as

$$\begin{aligned}\mathcal{L} = &\left(S_1 - S_1^* - S_1^* \ln\frac{S_1}{S_1^*}\right) + \left(S_2 - S_2^* - S_2^* \ln\frac{S_2}{S_2^*}\right) + \left(E - E^* - E^* \ln\frac{E}{E^*}\right) + \left(I - I^* - I^* \ln\frac{I}{I^*}\right) \\ &+ \left(A - A^* - A^* \ln\frac{A}{A^*}\right) + \left(Q - Q^* - Q^* \ln\frac{Q}{Q^*}\right).\end{aligned}$$

The time derivative of $\mathcal{L}$ is

$$\begin{aligned}D_\alpha\mathcal{L} = &\left(1 - \frac{S_1^*}{S_1}\right) D_\alpha S_1 + \left(1 - \frac{S_2^*}{S_2}\right) D_\alpha S_2 + \left(1 - \frac{E^*}{E}\right) D_\alpha E + \left(1 - \frac{I^*}{I}\right) D_\alpha I + \left(1 - \frac{A^*}{A}\right) D_\alpha A \\ &+ \left(1 - \frac{Q^*}{Q}\right) D_\alpha Q.\end{aligned} \tag{2.25}$$

Subtituted system (2.1) into equation (2.25) then obtained

$$\begin{aligned} D_\alpha \mathcal{L} = &\left(1-\frac{S_1^*}{S_1}\right)\left[(1-g)\mu-(\delta+\eta_1 I)S_1\right]+\left(1-\frac{S_2^*}{S_2}\right)\left[g\mu-(\delta+\eta_2 I)S_2\right]+\left(1-\frac{E^*}{E}\right)\left[(\eta_1 S_1+\eta_2 S_2)I\right.\\ &\left.-(\beta+\delta)E\right]+\left(1-\frac{I^*}{I}\right)\left[w\beta E-(\gamma+\delta+\theta)I\right]+\left(1-\frac{A^*}{A}\right)\left[(1-w)\beta E-(\rho+\delta)A\right]\\ &+\left(1-\frac{Q^*}{Q}\right)\left[\rho A+\gamma I-(\delta+\varepsilon)Q\right] \end{aligned} \tag{2.26}$$

At equilibrium, the following relations hold:

$$\begin{cases} (1-g)\mu &= (\delta+\eta_1 I^*)S_1^*,\\ g\mu &= (\delta+\eta_2 I^*)S_2^*,\\ \beta+\delta &= \frac{(\eta_1 S_1^*+\eta_2 S_2^*)I^*}{E^*},\\ \gamma+\delta+\theta &= \frac{w\beta E^*}{I^*},\\ \rho+\delta &= \frac{(1-w)\beta E^*}{A^*},\\ \delta+\varepsilon &= \frac{\rho A^*+\gamma I^*}{Q^*}. \end{cases} \tag{2.27}$$

Using the steady-state relation (2.27) in equations (2.26) and simplifying gives:

$$\begin{aligned} D_\alpha \mathcal{L} = &\delta S_1^*\left(2-\frac{S_1^*}{S_1}-\frac{S_1}{S_1^*}\right)+\delta S_2^*\left(2-\frac{S_2^*}{S_2}-\frac{S_2}{S_2^*}\right)\\ &+\eta_1 I^* S_1^*\left[\left(4-\frac{S_1^*}{S_1}-\frac{E}{E^*}-\frac{S_1 E^* I}{S_1^* E I^*}-\frac{I^*}{I}\right)-\left(2-\frac{I}{I^*}-\frac{I^*}{I}\right)\right]\\ &+\eta_2 I^* S_2^*\left[\left(4-\frac{S_2^*}{S_2}-\frac{E}{E^*}-\frac{S_2 E^* I}{S_2^* E I^*}-\frac{I^*}{I}\right)-\left(2-\frac{I}{I^*}-\frac{I^*}{I}\right)\right]\\ &+w\beta E^*\left[\left(3-\frac{E^*}{E}-\frac{E I^*}{E^* I}-\frac{I}{I^*}\right)-\left(2-\frac{E}{E^*}-\frac{E^*}{E}\right)\right]\\ &+(1-w)\beta E^*\left[\left(3-\frac{E^*}{E}-\frac{E A^*}{E^* A}-\frac{A}{A^*}\right)-\left(2-\frac{E}{E^*}-\frac{E^*}{E}\right)\right]\\ &+\rho A^*\left[\left(3-\frac{A^*}{A}-\frac{Q}{Q^*}-\frac{A Q^*}{A^* Q}\right)-\left(2-\frac{A}{A^*}-\frac{A^*}{A}\right)\right]\\ &+\gamma I^*\left[\left(3-\frac{I^*}{I}-\frac{Q}{Q^*}-\frac{I Q^*}{I^* Q}\right)-\left(2-\frac{I}{I^*}-\frac{I^*}{I}\right)\right]. \end{aligned} \tag{2.28}$$

Since the arithmetic mean is always greater than or equal to the geometric mean, this implies that:

$$\frac{I}{I^*}+\frac{I^*}{I}\geq 2, \frac{E}{E^*}+\frac{E^*}{E}\ \geq 2, \frac{A}{A^*}+\frac{A^*}{A}\geq 2,$$

and

$$\begin{gathered} \frac{S_1^*}{S_1}+\frac{S_1}{S_1^*}\geq 2, \frac{S_2^*}{S_2}+\frac{S_2}{S_2^*}\geq 2, \frac{S_1^*}{S_1}+\frac{E}{E^*}+\frac{S_1 E^* I}{S_1^* E I^*}+\frac{I^*}{I}\geq 4,\\ \frac{S_2^*}{S_2}+\frac{E}{E^*}+\frac{S_2 E^* I}{S_2^* E I^*}+\frac{I^*}{I}\geq 4, \frac{E^*}{E}+\frac{E I^*}{E^* I}+\frac{I}{I^*}\geq 3, \frac{E^*}{E}+\frac{E A^*}{E^* A}+\frac{A}{A^*}\geq 3,\\ \frac{A^*}{A}+\frac{Q}{Q^*}+\frac{A Q^*}{A^* Q}\geq 3, \frac{I^*}{I}+\frac{Q}{Q^*}+\frac{I Q^*}{I^* Q}\geq 3. \end{gathered}$$

Hence, this implies

$$\begin{aligned}
\delta S_1^* \left(2 - \frac{S_1^*}{S_1} - \frac{S_1}{S_1^*}\right) &\leq 0,\\
\delta S_2^* \left(2 - \frac{S_2^*}{S_2} - \frac{S_2}{S_2^*}\right) &\leq 0,\\
\eta_1 I^* S_1^* \left[\left(4 - \frac{S_1^*}{S_1} - \frac{E}{E^*} - \frac{S_1 E^* I}{S_1^* E I^*} - \frac{I^*}{I}\right) - \left(2 - \frac{I}{I^*} - \frac{I^*}{I}\right)\right] &\leq 0,\\
\eta_2 I^* S_2^* \left[\left(4 - \frac{S_2^*}{S_2} - \frac{E}{E^*} - \frac{S_2 E^* I}{S_2^* E I^*} - \frac{I^*}{I}\right) - \left(2 - \frac{I}{I^*} - \frac{I^*}{I}\right)\right] &\leq 0,\\
w\beta E^* \left[\left(3 - \frac{E^*}{E} - \frac{E I^*}{E^* I} - \frac{I}{I^*}\right) - \left(2 - \frac{E}{E^*} - \frac{E^*}{E}\right)\right] &\leq 0,\\
(1-w)\beta E^* \left[\left(3 - \frac{E^*}{E} - \frac{E A^*}{E^* A} - \frac{A}{A^*}\right) - \left(2 - \frac{E}{E^*} - \frac{E^*}{E}\right)\right] &\leq 0,\\
\rho A^* \left[\left(3 - \frac{A^*}{A} - \frac{Q}{Q^*} - \frac{A Q^*}{A^* Q}\right) - \left(2 - \frac{A}{A^*} - \frac{A^*}{A}\right)\right] &\leq 0,\\
\gamma I^* \left[\left(3 - \frac{I^*}{I} - \frac{Q}{Q^*} - \frac{I Q^*}{I^* Q}\right) - \left(2 - \frac{I}{I^*} - \frac{I^*}{I}\right)\right] &\leq 0.
\end{aligned}$$

Clearly $D_\alpha \mathcal{L} \leq 0$, with $D_\alpha \mathcal{L} = 0$ if and only if $S_1 = S_1^*$, $S_2 = S_2^*$, $E = E^*$, $I = I^*$, $A = A^*$, and $Q = Q^*$. The endemic equilibrium is special and unique if $\mathcal{R}_0 > 1$, and the singleton set $\{\varepsilon^*\}$ is the largest compact invariant set in

$$\{(D^\alpha S_1(t), D^\alpha S_2(t), D^\alpha E(t), D^\alpha I(t), D^\alpha A(t), D^\alpha Q(t)) \in \Omega : D_\alpha \mathcal{L}(t) = 0\}.$$

Based on LaSalle's invariance principle (Lemma 2.7), ε^* is globally asymptotically stable in the interior of region $\Omega \setminus \Omega_0$ if $\mathcal{R}_0 > 1$. □

3. Results and Discussion

3.1. Parameter Estimation

The number of infected cases in model (2.1) were obtained from annual confirmed diphtheria case data in Indonesia, taken from [36, 39]. The data used covers the years 2012 to 2023, with model projections for 2024 to 2028. In 2012, the population of Indonesia was 4,670,332, with 1,192 infected individuals. Meanwhile, the initial values in model (2.1) are

$$(S_{1_0}, S_{2_0}, E_0, I_0, A_0, Q_0, R_0) = (4670332; 24941078; 60000; 1192; 1000; 6000; 7478).$$

The determination of numerical solutions was carried out using the predictor-corrector method derived by [18]. The scheme of the method has an accuracy level of $O(h^{1+\alpha})$ when $0 < \alpha < 1$. Based on research from [18], if the value of α is larger, then the order of the predictor-corrector scheme is also getting larger. This scheme has the ability to provide solutions that are aligned with the dynamics of analytics, especially if the step size is relatively small.

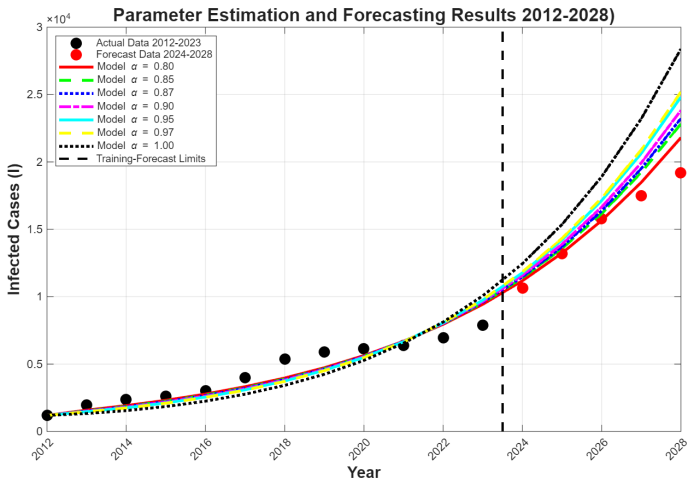

Figure 2: Numerical solutions from actual data and forecasting of diphtheria cases from 2012 to 2028

By using model (2.1) together with the first-order model on diphtheria data, the eleven parameters can be estimated using the nonlinear least squares (NLS) method, allowing for a comparison of each model with the actual data and for forecasting diphtheria cases. The values of α considered in this model are $\alpha = 0.8, 0.85, 0.87, 0.9$. To evaluate the best model, this study employs the Root Mean Square Error (RMSE), which is expressed as:

$$\text{RMSE} = \sqrt{\frac{\sum_{i=1}^{N}(y_i - \hat{y}_i)^2}{N}}$$

with N, y_i, and $\hat{y}_i$ are the sum of data, actual data, and prediction data using fifth-order and fourth-order Runge-Kutta in period i. The estimated parameter values of model (2.1) are shown in Table 2 as follows:

Table 2: Parameter values for each α

Parameter	**Order** α						
	$\alpha = 0.8$	$\alpha = 0.85$	$\alpha = 0.87$	$\alpha = 0.9$	$\alpha = 0.95$	$\alpha = 0.97$	$\alpha = 1$
g	0.080921	0.081484	0.0808	0.080971	0.081453	0.08121	0.18
μ	0.09	0.09	0.09	0.09	0.09	0.09	0.09
δ	0.0141	0.0141	0.0141	0.0141	0.0141	0.0141	0.0141
η_1	0.12022	0.12	0.12023	0.12001	0.12008	0.12001	0.12
η_2	0.1	0.1	0.1	0.1	0.1	0.1	0.1
β	0.028267	0.027374	0.02698	0.026418	0.025444	0.025053	0.00833
γ	0.000302	0.000329	0.0003	0.0003	0.0003	0.0003	0.0003
θ	0.003001	0.003022	0.003	0.003	0.003	0.003	0.003
ε	0.055	0.055	0.055	0.055	0.055	0.055	0.01535
w	0.25009	0.25	0.25008	0.25	0.25003	0.25003	0.25
ρ	0.012	0.012	0.012	0.012	0.012	0.012	0.00309

Based on Figure 2, the solution curves with values of $\alpha = 0.8, 0.85, 0.87, 0.9$ are able to follow the trend of the actual data quite well, thus accurately depicting the trend of diphtheria cases from 2012 to 2028, while the model with $\alpha = 0.97$ shows a considerable deviation from the data, particularly for diphtheria cases from 2026 to 2028. Nevertheless, the assessment shown in Figure 2 is not sufficient to evaluate the model results overall, making it necessary to calculate the Root Mean Square Error (RMSE) to present the calibration obtained using the least square method, which are shown in Table 3. For diphtheria data, the model with $\alpha = 0.8$ produces the best result with the smallest RMSE value, followed by $\alpha = 0.85, 0.87$, and

0.9. Meanwhile, the models with $\alpha = 0.97$ and 1 yield the largest RMSE compared to the other α values. This is consistent with the assessment shown by the solution curves in Figure 2.

Table 3: RMSE results for each α value

$\alpha = 0.8$	$\alpha = 0.85$	$\alpha = 0.87$	$\alpha = 0.9$	$\alpha = 0.95$	$\alpha = 0.97$	$\alpha = 1$
822.42	879.12	901.26	932.97	984.26	1003.91	1200.00

According to Table 3, it can be seen that the model with $\alpha = 0.8$ has the smallest RMSE at the numerical solution calculated using the fifth-order and fourth-order Runge-Kutta methods, making this model provide better forecasts compared to the other α values. This is followed by the models with $\alpha = 0.85$, 0.87 and 0.9. Thus, the annual confirmed diphtheria cases can be associated with the basic reproduction number. The evaluation results for $\mathcal{R}_0$ for the calibration of model (2.1) use the same formula as the first-order model with the least squares method. For $\alpha = 0.8$, the basic reproduction number obtained is $7.2964 > 1$. This value indicates that diphtheria cases are always present. To provide a more rigorous justification for our parameter estimation approach, we compared our method with recent diphtheria modeling studies. For instance, the Extended Kalman Filter applied to West Java diphtheria data demonstrated good performance based on RMSE metrics [21]. Similarly, parameter estimation for the Rohingya refugee camp outbreak utilized numerical fitting techniques to obtain $\mathcal{R}_0 = 5.86$. While absolute RMSE values differ due to spatial and temporal scales, our fractional-order model with $\alpha = 0.8$ achieves a lower RMSE (822.42) compared to the integer-order case ($\alpha = 1$, RMSE = 1200.00), consistent with findings that fractional models provide better fit for diseases with long-term memory effects like diphtheria. Therefore, diphtheria cases have the potential to become endemic during the calibration period. This very high $\mathcal{R}_0$ value emphasizes that strong public health interventions with the support of vaccination and quarantine can reduce the potential spread of the disease.

3.2. Sensitivity Analysis of Model Parameters

The parameters in model (2.1) each affect the effective reproduction number differently. To identify which parameters significantly influence $\mathcal{R}_0$, a sensitivity analysis is performed using the approach described in [22].

Definition 3.1. The normalized forward sensitivity index of $\mathcal{R}_0$, which is differentiable with respect to a fundamental parameter τ, is defined as: $T_\tau^{\mathcal{R}_0} = \frac{\partial \mathcal{R}_0}{\partial \tau} \times \frac{\tau}{\mathcal{R}_0}$ [22]:

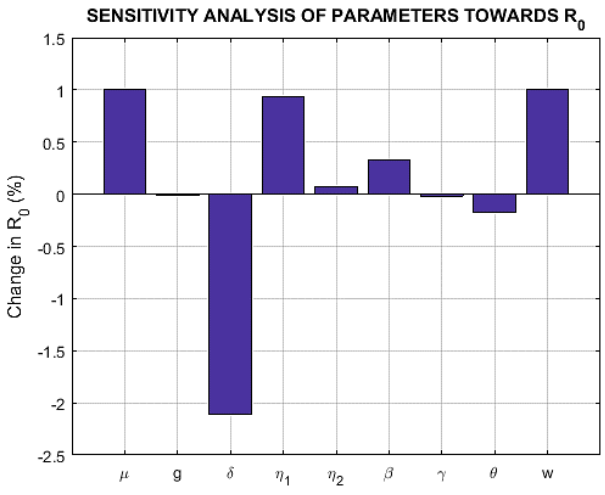

Figure 3: Parameter sensitivity analysis on $\mathcal{R}_0$ in diphtheria cases from 2012 to 2028

We determine the sensitivity of each fundamental parameter in $\mathcal{R}_0$ as follows:

$$\begin{cases} \mathcal{R}_0 = \dfrac{w(\eta_1(1-g)+\eta_2 g)\beta\mu}{\delta(\beta+\delta)(\gamma+\theta+\delta)}, \\ T_\beta^{\mathcal{R}_0} = \dfrac{\partial \mathcal{R}_0}{\partial \beta} \times \dfrac{\beta}{\mathcal{R}_0} = \dfrac{\delta}{\beta+\delta}, \\ T_{\eta_1}^{\mathcal{R}_0} = \dfrac{\partial \mathcal{R}_0}{\partial \eta_1} \times \dfrac{\eta_1}{\mathcal{R}_0} = \dfrac{\eta_1(1-g)}{\eta_1(1-g)+\eta_2 g}, \\ T_{\eta_2}^{\mathcal{R}_0} = \dfrac{\partial \mathcal{R}_0}{\partial \eta_2} \times \dfrac{\eta_2}{\mathcal{R}_0} = \dfrac{\eta_2 g}{\eta_1(1-g)+\eta_2 g}, \\ T_\mu^{\mathcal{R}_0} = \dfrac{\partial \mathcal{R}_0}{\partial \mu} \times \dfrac{\mu}{\mathcal{R}_0} = +1, \\ T_\delta^{\mathcal{R}_0} = \dfrac{\partial \mathcal{R}_0}{\partial \delta} \times \dfrac{\delta}{\mathcal{R}_0} = -\left(1 + \dfrac{\delta}{\beta+\delta} + \dfrac{\delta}{\gamma+\theta+\delta}\right), \\ T_\gamma^{\mathcal{R}_0} = \dfrac{\partial \mathcal{R}_0}{\partial \gamma} \times \dfrac{\gamma}{\mathcal{R}_0} = -\dfrac{\gamma}{\gamma+\theta+\delta}, \\ T_\theta^{\mathcal{R}_0} = \dfrac{\partial \mathcal{R}_0}{\partial \theta} \times \dfrac{\theta}{\mathcal{R}_0} = -\dfrac{\theta}{\gamma+\theta+\delta}, \\ T_w^{\mathcal{R}_0} = \dfrac{\partial \mathcal{R}_0}{\partial w} \times \dfrac{w}{\mathcal{R}_0} = 1. \end{cases}$$

.

Based on the results of the sensitivity analysis of the parameters on the basic reproduction number $\mathcal{R}_0$ shown in Figure 3, it was identified that each parameter has a different influence on the potential spread of the disease when a 1% change is made. The parameter δ (natural death rate) shows the most significant effect with a decrease in $\mathcal{R}_0$ of -2.11%, indicating a strong inverse relationship. Meanwhile, the parameters μ (natural growth rate) and w (proportion of infected individuals who are symptomatic) are the most sensitive parameters with the highest positive effect, where a 1% increase in these parameters results in a 1% increase in $\mathcal{R}_0$. The parameter η_1 (probability of interaction between the vulnerable subpopulation and the infected subpopulation) has a significant effect with a change in $\mathcal{R}_0$ of $+0.93\%$, followed by β (infection rate) with $+0.33\%$. Therefore, controlling sources of infection, such as interactions between subpopulations, needs to be carried out, leading to a reduction in diphtheria cases. The following details show the results of changes in $\mathcal{R}_0$ and their effects on each parameter, as presented in Table 4.

Table 4: Sensitivity Index of Parameters

Notation	**Sensitivity Index**
μ	1.0000
g	-0.0138
δ	-2.1116
η_1	0.9318
η_2	0.0682
β	0.3306
γ	-0.0174
θ	-0.1721
w	1.0000

3.3. Numerical Simulation

Based on the numerical simulation graph in Figure 4 for diphtheria cases from 2012–2023, the interpretation of subpopulation dynamics shows differences in patterns for each value of α. For $\alpha = 0.8$, the curves

for the exposed (E), infected (I), and quarantined (Q) subpopulations in Figures 4a, 4b, and 4d show a gradual and elongated pattern throughout the simulation period. This illustrates the slow movement of the healthcare system; the diphtheria outbreak does not spread suddenly but occurs slowly and continuously over many years. Meanwhile, the subpopulation of asymptomatic infected individuals (A) reached the highest cases as seen in Figure 4c, indicating that the contribution of asymptomatic diphtheria cases has a significant impact on the increase in disease spread. Whereas, Figure 4e shows that the recovered subpopulation (R) only increased significantly in the later period after experiencing a prolonged outbreak.

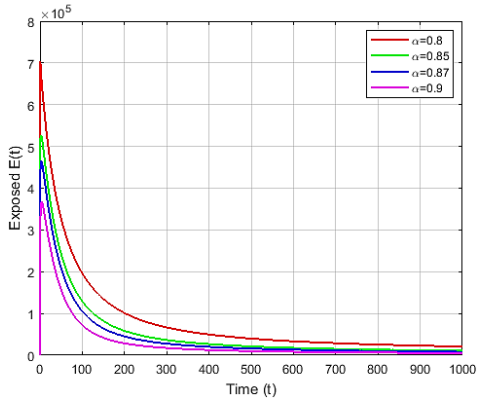

(a) Exposed subpopulation (E)

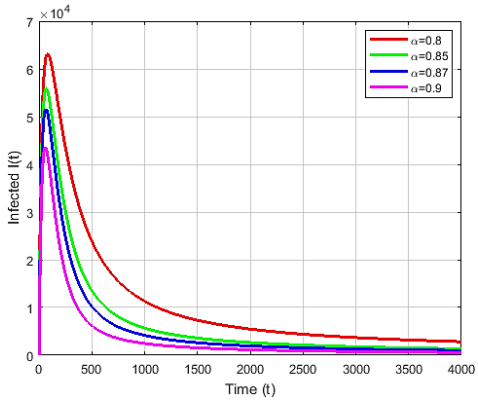

(b) Infected subpopulation (I)

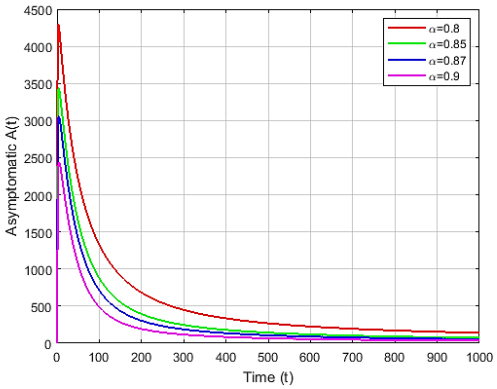

(c) Asymptomatic infected subpopulation (A)

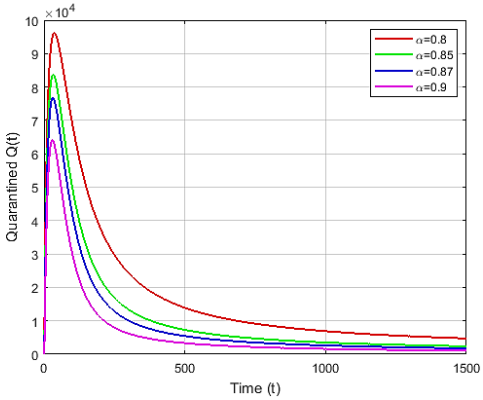

(d) Quarantined subpopulation (Q)

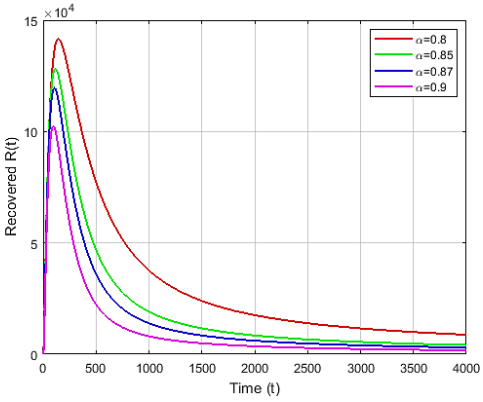

(e) Recovered subpopulation (R)

Figure 4: Numerical Solution of Model (2.1) with variations in α values.

At $\alpha = 0.85$, the E and I curves are flatter with lower peaks (see Figures 4a and 4b), but their

duration is longer than at $\alpha = 0.8$, indicating that the outbreak did not spread significantly but continued persistently. Meanwhile, the asymptomatic infected subpopulation (A) shown in Figure 4c tends to be high and persistent, meaning that asymptomatic cases dominate diphtheria cases from 2012 to 2023. After the quarantined subpopulation (Q) began to be implemented (see Figure 4d), thereby reducing the rate of transmission. Meanwhile, the recovered subpopulation (R) in Figure 4e increases steadily but slowly in line with the longer duration of the outbreak. For the variation $\alpha = 0.87$, disease control is already better. Although the outbreak is still spreading, it is detected earlier. The number of infected individuals (A) starts to decline, as seen in Figure 4c, and quarantine is implemented more quickly, thereby reducing the transmission rate. Additionally, more individuals recover, and this occurs in a shorter timeframe.

For $\alpha = 0.9$, the health system operates at optimal speed. The outbreak spiked at the beginning of the period, but was quickly resolved through strict quarantine, continuous contact tracing, and early detection of disease transmission. Furthermore, subpopulation A was relatively low and declined after reaching its peak (see Figure 4c). In addition, subpopulation R increases steadily as shown in Figure 4e, so that treatment was successful in a relatively short time. Overall, it can be concluded that the lower the value of α, the longer the duration of the dynamics of diphtheria case spread. Conversely, if α is higher, the decline in diphtheria cases is faster and more effective.

3.4. Variations in the Basic Reproduction Number

Based on the infected subpopulation (I) of diphtheria cases from 2012 to 2023 shown in Figure 5, the given I subpopulation graph illustrates how infection dynamics are influenced by transmission parameters, namely the parameter β (transmission rate), η_1 (probability of interaction between highly susceptible subpopulation and infected subpopulation), η_2 (probability of interaction between susceptible subpopulation and infected subpopulation), and w (proportion of symptomatic infected subpopulation).

From the analysis, when the parameter values are higher, as in the first case in each graph, that is when $\beta = 0.09$, $\eta_1 = 0.09$, $\eta_2 = 0.08$, and $w = 0.07$, the value of $\mathcal{R}_0$ is also higher, as in the first case where $\mathcal{R}_0$ is 1.89. This is seen in the increasing subpopulation I curve moving away from 0, leading to a widespread and uncontrolled diphtheria outbreak. Conversely, when the parameter values decrease, as in the fourth case with $\beta = 0.05$, $\eta_1 = 0.04$, $\eta_2 = 0.05$ and $w = 0.03$, $\mathcal{R}_0$ can be suppressed to a value of 0.35 in the fourth case, so that $\mathcal{R}_0 < 1$. This means the curve approaches zero, indicating successful outbreak control.

In addition, the timing of diphtheria case spread is also influenced by the value of α, as seen in Figures 5a–5f. A model with a value of $\alpha = 1$ shows the sharpest and fastest movement of the diphtheria outbreak, as shown in Figure 5f. The smaller the value of α, the smoother and more gradual the graph. In this context, diphtheria is a disease with immunization coverage whose effects occur in the long term, so using a model with $\alpha = 0.8$, whose dynamics can be seen in Figure 5a, provides a more realistic picture for planning other policies in controlling diphtheria cases.

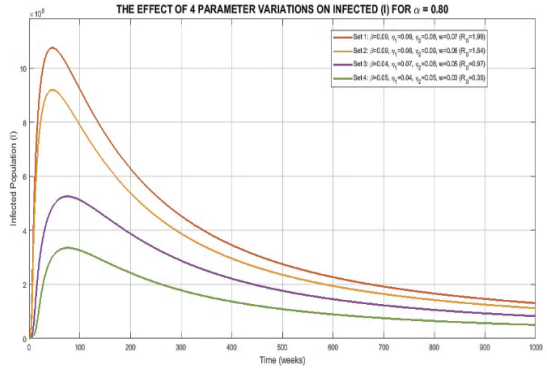

(a) Variation of $\mathcal{R}_0$ for $\alpha = 0.8$

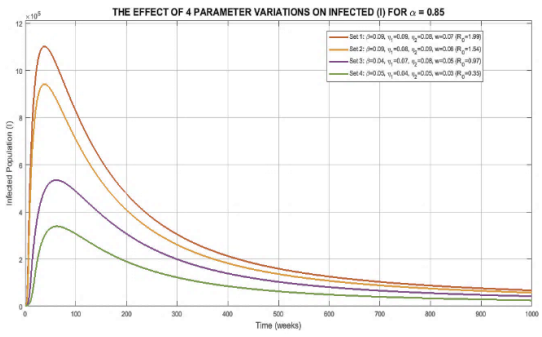

(b) Variation of $\mathcal{R}_0$ for $\alpha = 0.85$

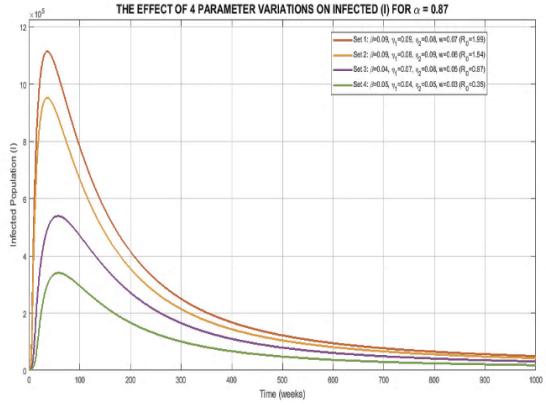

(c) Variation of $\mathcal{R}_0$ for $\alpha = 0.87$

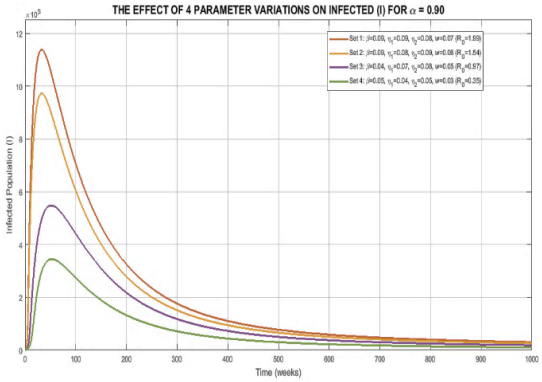

(d) Variation of $\mathcal{R}_0$ for $\alpha = 0.9$

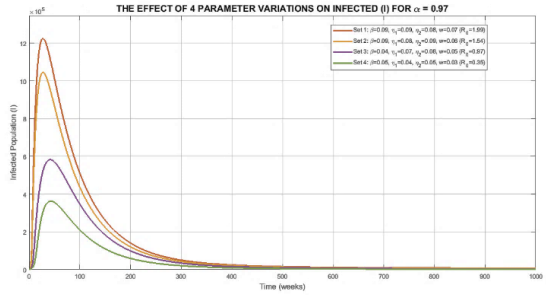

(e) Variation of $\mathcal{R}_0$ for $\alpha = 0.97$

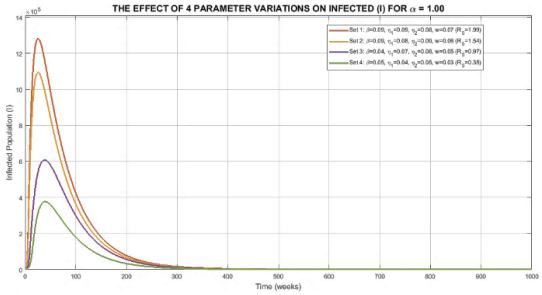

(f) Variation of $\mathcal{R}_0$ for $\alpha = 1$

Figure 5: Numerical solutions of model (2.1) showing the infected subpopulation (I) with variations in $\mathcal{R}_0$ for different values of α.

Based on the asymptomatic infected subpopulation (A) of diphtheria cases from 2012 to 2023 shown in Figure 6, the graph of subpopulation A shows how the dynamics of infection are influenced by four main parameters, namely parameter β (transmission rate), η_1 (the probability of interaction between the highly susceptible subpopulation and the infected subpopulation), η_2 (the probability of interaction between the susceptible subpopulation and the infected subpopulation), and w (the proportion of the infected subpopulation that is symptomatic). Figures 6a through 6f each illustrate the response of subpopulation A to variations in the α value (0.8, 0.85, 0.87, 0.9, 0.97, and 1) under different combinations of these parameters. When the parameter values are higher, as in the first case in the graph when $\beta = 0.08$, $\eta_1 = 0.08$, $\eta_2 = 0.08$, and $w = 0.07$, the $\mathcal{R}_0$ value is also higher, as in the first case where the $\mathcal{R}_0$ value is 1.99. This is seen in the curve of subpopulation A, which increases and moves away from 0, resulting in an outbreak of diphtheria cases without symptoms that is widespread and uncontrolled. Conversely, if the parameter values decrease, as in the fourth case with $\beta = 0.05$, $\eta_1 = 0.04$, $\eta_2 = 0.05$ and $w = 0.03$, then $\mathcal{R}_0$ can be suppressed and produce a value of 0.35 in the fourth case, so that $\mathcal{R}_0 < 1$, which means that the curve approaches zero, indicating successful outbreak control.

In addition, the spread time of diphtheria cases is also influenced by the α value. A model with a value of $\alpha = 1$ in Figure 6f shows the sharpest and fastest movement of the diphtheria outbreak. The smaller the α value, the smoother and flatter the graph. In this context, asymptomatic infected cases of diphtheria are a source of transmission that is difficult to trace, so it takes a long time to detect the transmission. Therefore, $\alpha = 0.8$ provides a more realistic picture for planning other policies to control diphtheria cases.

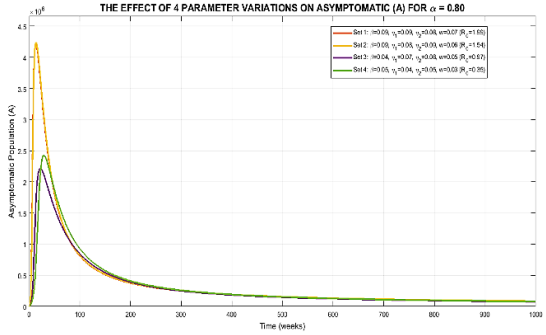

(a) Variations in $\mathcal{R}_0$ for $\alpha = 0.8$

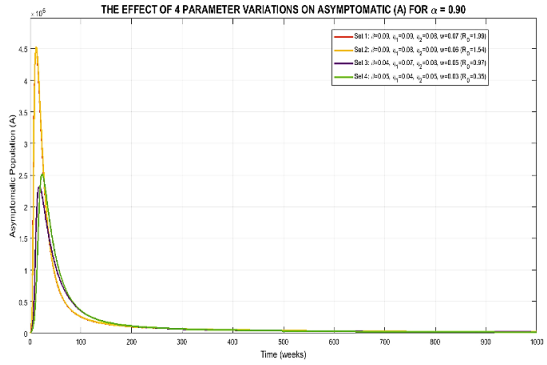

(b) Variations in $\mathcal{R}_0$ for $\alpha = 0.85$

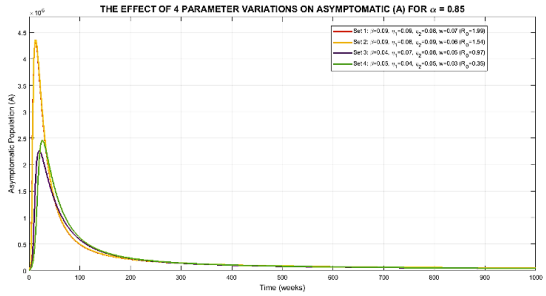

(c) Variation of $\mathcal{R}_0$ for $\alpha = 0.87$

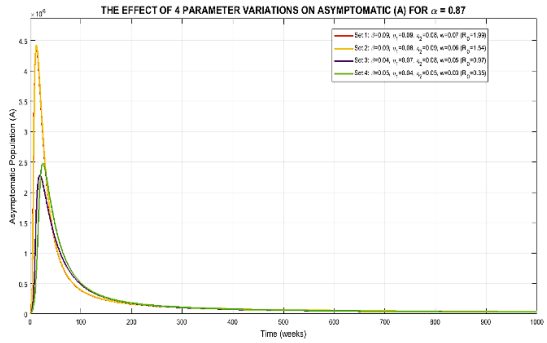

(d) Variation of $\mathcal{R}_0$ for $\alpha = 0.9$

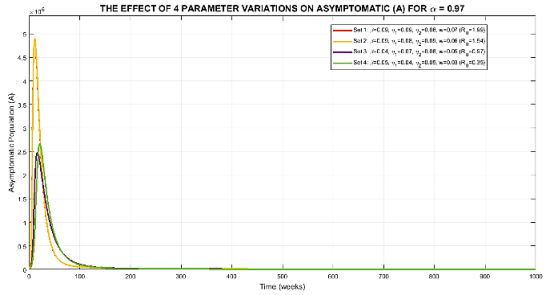

(e) Variation of $\mathcal{R}_0$ for $\alpha = 0.97$

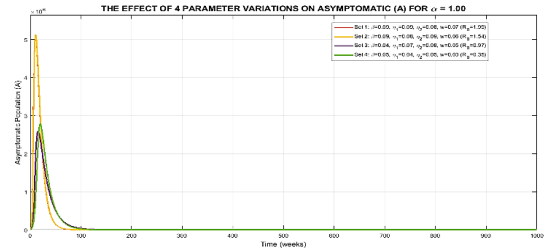

(f) Variation of $\mathcal{R}_0$ for $\alpha = 1$

Figure 6: Numerical solutions of model (2.1) between the asymptomatic infected subpopulation (A) with variations in $\mathcal{R}_0$ for each different value of α.

3.5. Parameter Variations

3.5.1. Variations η_1

Based on the analysis of the η_1 parameter variation graph shown in Figure 7, when η_1 is 0.05, it produces an $\mathcal{R}_0$ of **0.1596**, which indicates a disease-free condition, but with a significant final infected and exposed population. Next, when η_1 is increased to 0.06, the $\mathcal{R}_0$ value increases to 0.1867, still in the disease-free condition, followed by a decrease in the susceptible population S_1, S_2 and an increase in the number of recovered individuals (R) as seen in Figures 7a–7b and Figure 7g. The $\mathcal{R}_0$ value continues to increase at $\eta_1 = 0.2$ to **0.5666**, but remains below 1. At $\eta_1 = 0.8$, the $\mathcal{R}_0$ value jumps to 2.1946, indicating an endemic condition, and becomes even higher at $\eta_1 = 0.9$ with an $\mathcal{R}_0$ of 2.4660. At these endemic values, the susceptible population decreases further as it shifts to the exposed state visualized in Figure 7c.

The larger the η_1 value, the larger the E (exposed) population because a higher transmission rate causes more susceptible individuals to be exposed. The I (symptomatically infected) and A (asymptomatically infected) populations also increase as exposed individuals enter the active infection period. The Q (quarantined/isolated) population also increases along with the rise in the number of infected cases requiring treatment. The R (recovered) population also increases as η_1 increases, especially during endemic conditions ($\mathcal{R}_0 > 1$). This occurs because with a high transmission rate, the number of patients being treated increases significantly, so even though the spread is wider, the healthcare system still produces a large number of recoveries from patients who successfully heal. Conversely, when η_1 is reduced, the curve tends to approach 0, meaning $\mathcal{R}_0 < 1$ and the disease is no longer able to spread, eventually becoming extinct.

Thus, efforts to suppress the spread of disease can be carried out by expanding vaccination, implementing strict quarantine, and reducing direct physical interaction. If this is done and successful, the basic number can be reduced to near 0, which means that no one will transmit the disease to others. As a result, the spread of diphtheria can be controlled and stopped in the long term.

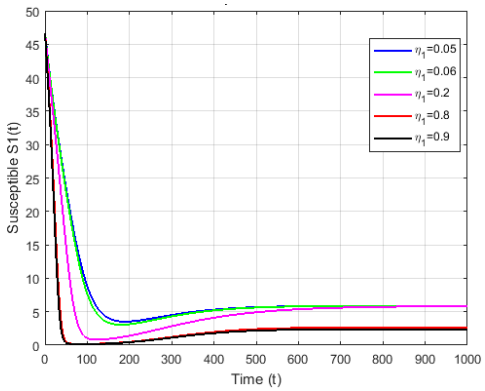

(a) Variation of η_1 against S_1

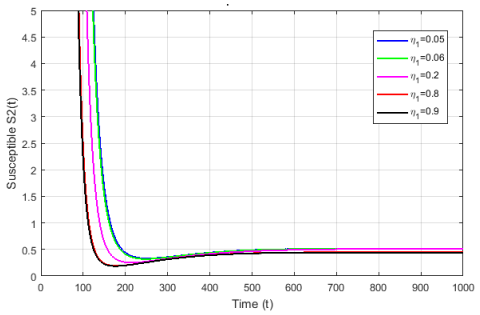

(b) Variation of η_1 against S_2

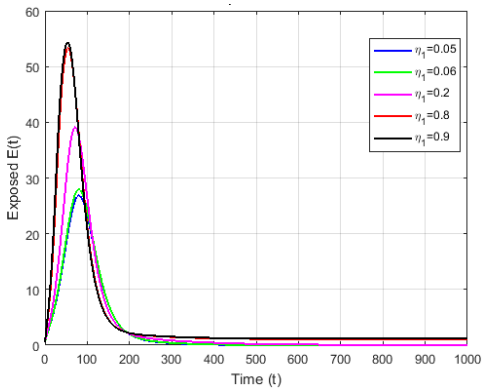

(c) Variation of η_1 against E

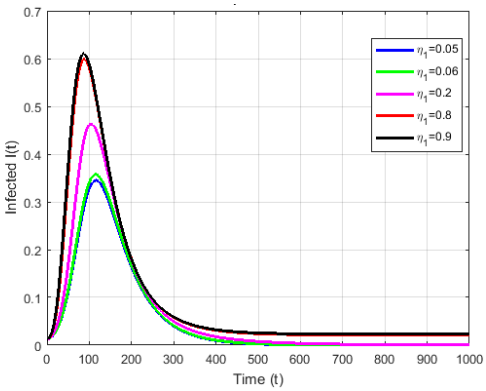

(d) Variation of η_1 against I

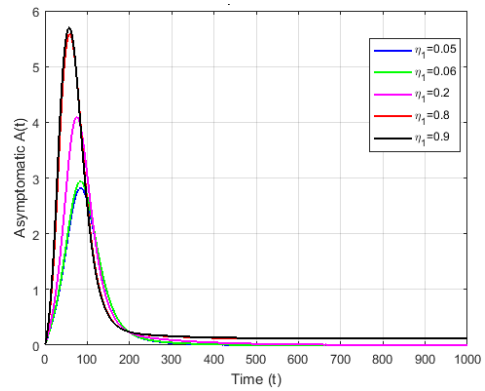

(e) Variation of η_1 against A

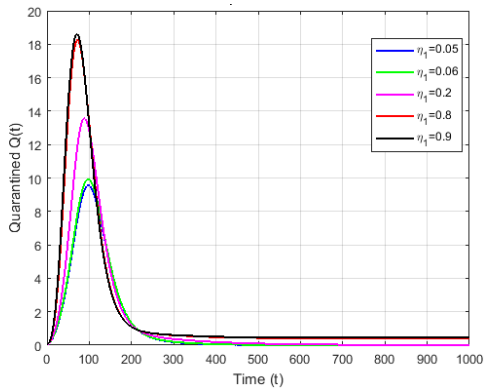

(f) Variation of η_1 against Q

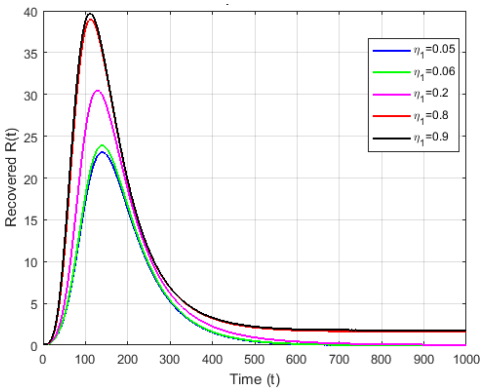

(g) Variation of η_1 against R

Figure 7: Numerical solution of model (2.1) parameter variation η_1.

3.5.2. Variations η_2

Based on the results of the diphtheria model simulation shown in Figure 8, the variation in the η_2 parameter has five different values, namely 0.1, 0.3, 0.5, 0.7, and 0.9. Each parameter value of η_2 has an impact on the basic reproduction number $\mathcal{R}_0$. When η_2 is 0.1, the value of $\mathcal{R}_0$ is 0.4231 (disease-free condition), then it increases to 0.7809 at $\eta_2 = 0.3$, reaches 1.1386 at $\eta_2 = 0.5$ (disease spread begins), and continues to rise to 1.4964 and 1.8541 at $\eta_2 = 0.7$ and 0.9, indicating that the transmission situation is getting stronger and has the potential to cause a wider outbreak. The larger the value of η_2, the larger the number of subpopulations E (exposed), I (infected), A (asymptomatic), Q (quarantined), and R (recovered). The reason is that an increase in η_2 increases the effective contact rate between S_2 and I. So that more vaccinated susceptible individuals are exposed and move to the E compartment. From E, individuals develop into active infected cases (I), and some others become asymptomatic cases (A). The increase in the number of infected cases (I) and exposed individuals (E) causes more individuals to be quarantined (Q). Regarding the subpopulation R (recovered), an increase in η_2 also causes the recovered population to increase because when η_2 is large, the situation becomes endemic with a high transmission rate, so many patients are treated and successfully recover. This can be seen from the simulation data, when $\eta_2 = 0.1$, the R subpopulation is 41.0309; at $\eta_2 = 0.3$ it increases to 43.2973; and at $\eta_2 = 0.9$ it reaches 44.1359 (Figure 8g). Furthermore, the I subpopulation continues to increase from 0.2920 ($\eta_2 = 0.1$) to 0.3120 ($\eta_2 = 0.9$) (Figure 8d). A similar increase is also observed in the subpopulations E (Figure 8c), A (Figure 8e), and Q (Figure 8f) as η_2 increases. This indicates that reducing η_2 through quarantine and reducing risky contact is very important to suppress the number of infected cases and prevent endemic conditions.

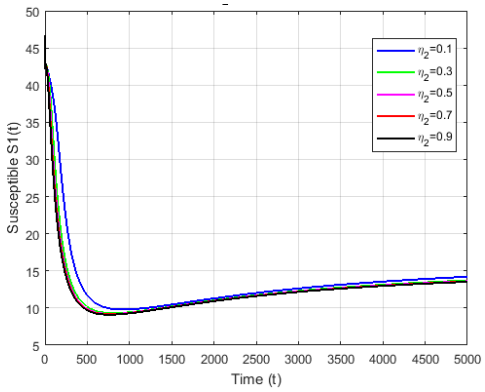

(a) Variation of η_2 against S_1

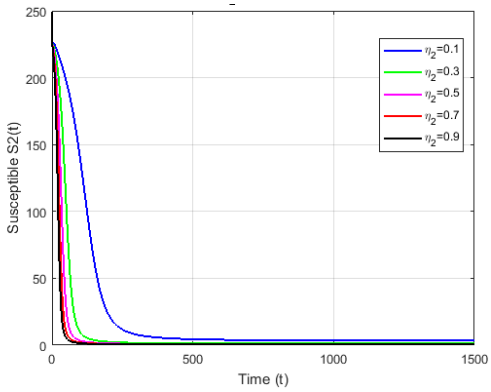

(b) Variation of η_2 against S_2

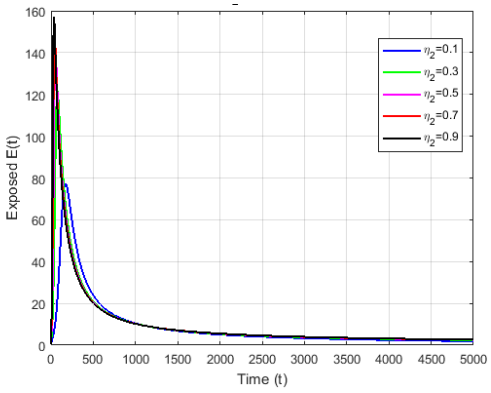

(c) Variation of η_2 against E

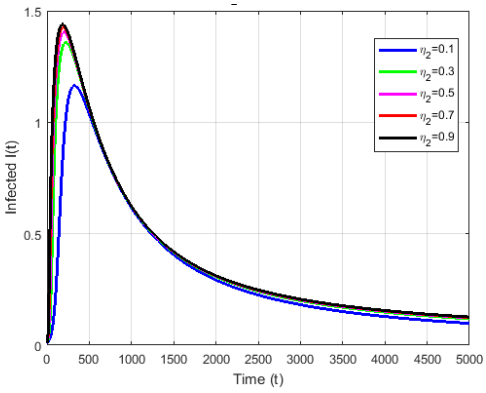

(d) Variation of η_2 against I

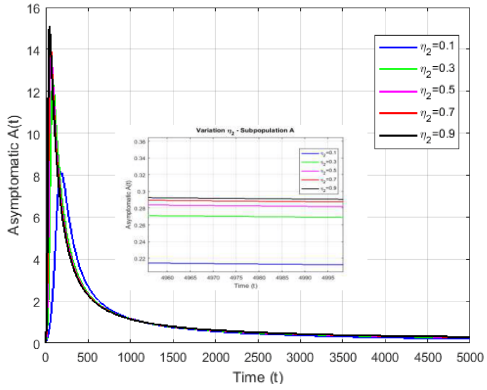

(e) Variation of η_2 against A

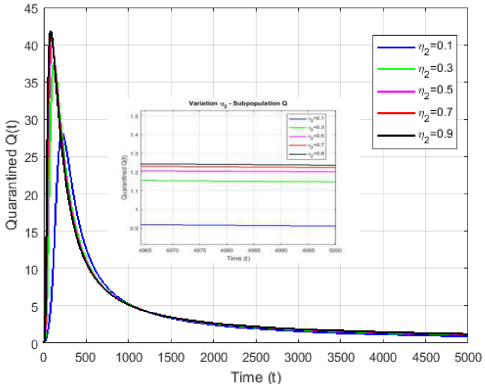

(f) Variation of η_2 against Q

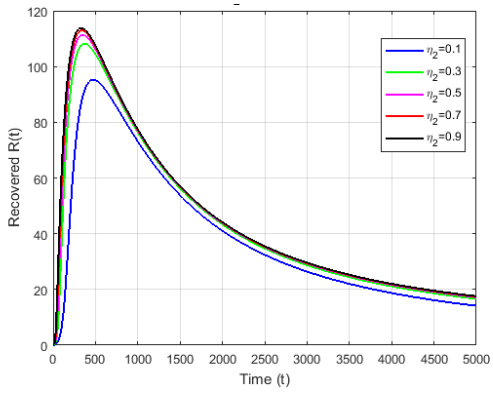

(g) Variation of η_2 against R

Figure 8: Numerical solution of model (2.1) parameter variation η_2.

3.5.3. Variations w

Based on the results of the diphtheria model simulation shown in Figure 9, the variation in the w parameter has five different values, namely 0.1, 0.3, 0.5, 0.7, and 0.9. The simulation data shows that the higher the value of w, the more symptomatic infected subpopulations there are, so the basic reproduction number $\mathcal{R}_0$ increases dramatically, from 0.4709 at $w = 0.1$ to 4.2384 at $w = 0.9$. This indicates that outbreaks with a higher proportion of symptomatic cases are much more contagious. An increase in w results in a decrease in the number of susceptible subpopulations at the end of the simulation. In Figure 9a (variation of w against S_1) and Figure 9b (variation of w against S_2), subpopulation S_1 decreases from 5.87 to 2.13, while S_2 also decreases from 0.51 to 0.3. This means that outbreaks with many symptomatic cases cause the disease to spread, so that more subpopulations are exposed and leave the susceptible subpopulation.

In the S_1 and S_2 graphs, the variation in w shows that the decline in the susceptible population occurs more rapidly as the value of w increases. Meanwhile, the infected subpopulation (I) displayed in Figure 9d exhibits a significant surge, the number experienced a significant surge, rising from 0 to 2.06. Furthermore, the exposed subpopulation (E) shown in Figure 9c also increased from 0 to 1.41, which means that the chain accelerated very quickly. However, the number of the asymptomatic subpopulation (A) in Figure 9e remains very low, indicating that if almost all infections are symptomatic, then asymptomatic cases will be very few. The quarantined (Q) and recovered (R) subpopulations (see Figures 9f–9g) peak when the value of w is 0.1, namely 0.18 and 0.69. The graphs then decline for higher values of w. This indicates that when the proportion of symptomatic cases increases, namely when $w = 0.7$ and 0.9, the spread occurs too quickly and the large number of cases can disrupt treatment, resulting in fewer members of the S_1 subpopulation being successfully quarantined and a lower number of recoveries.

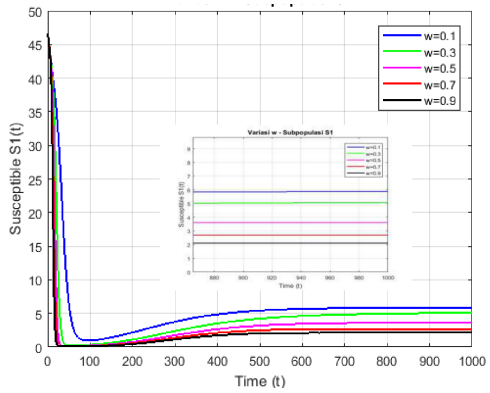

(a) Variation of w against S_1

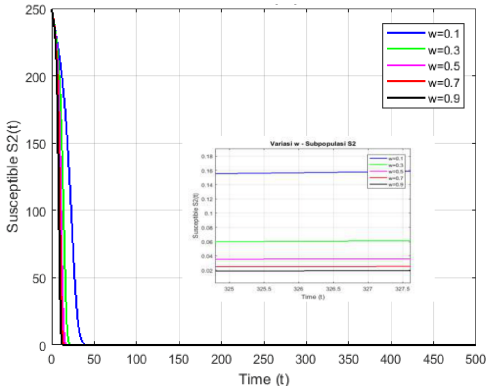

(b) Variation of w against S_2

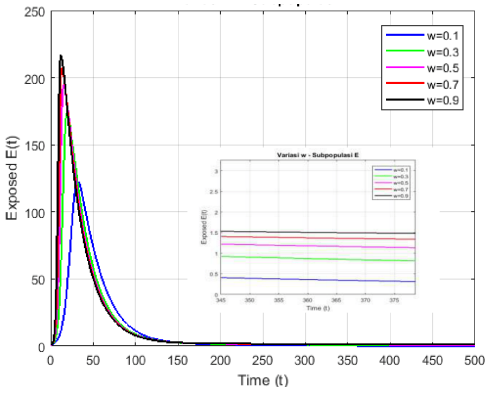

(c) Variation of w against E

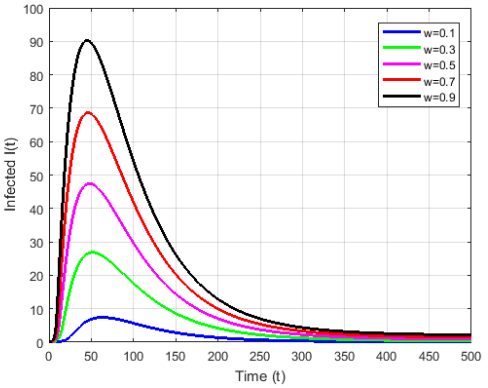

(d) Variation of w against I

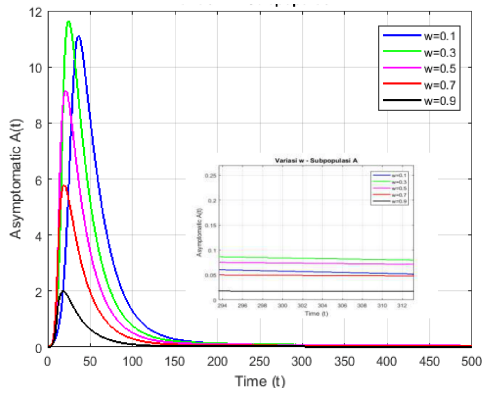

(e) Variation of w against A

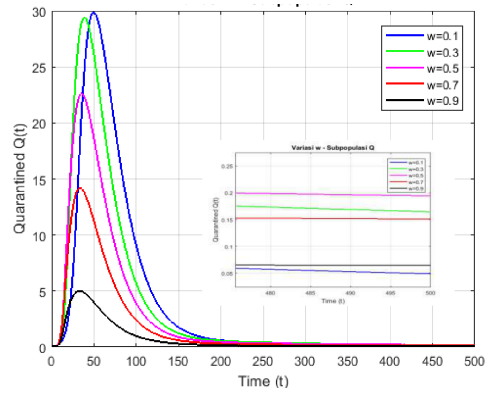

(f) Variation of w against Q

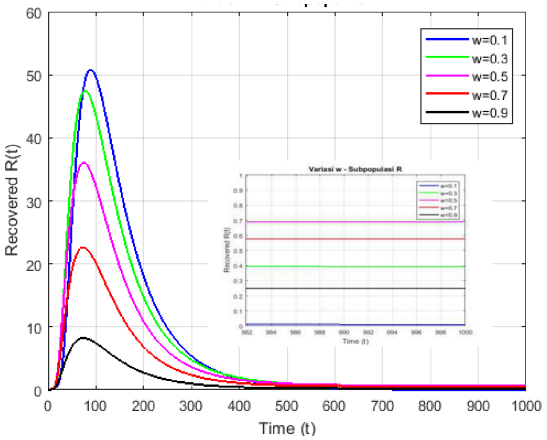

(g) Variation of w against R

Figure 9: Numerical solution of model (2.1) parameter variation w.

3.5.4. Variations β

Based on the results of the diphtheria model simulation shown in Figure 10, the variation in the β parameter has five different values, namely 0.09, 0.1, 0.2, 0.5, and 0.9. The graph shows that an increase in β causes a significant change in the number of infected subpopulations I and A, and other subpopulations are also affected, namely E (exposed), Q (quarantined), and R (recovered) (see Figures 10c–10g). The larger the value of β, the larger the subpopulations I, A, Q, and R. An increase in β leads to a higher disease transmission rate, so more susceptible individuals are exposed and eventually enter the infection stage. Consequently, subpopulation I increases because more individuals show clinical symptoms, while subpopulation A also increases as part of the total infected individuals. The rise in infected cases then drives an increase in subpopulation Q, as more patients are detected and placed in quarantine to prevent further transmission. Furthermore, in subpopulation R (recovered), the larger the value of β, which also reflects the disease progression rate from the exposed stage (E) to the infected stage (I), the faster the disease cycle progresses. Additionally, during an outbreak or endemic condition, more patients are treated and successfully recover, so the accumulation of recovered individuals also increases.

For β is 0.09, the value of $\mathcal{R}_0 < 1$, which is 0.9874, indicating that the disease does not spread widely. However, for β increases to 0.2, $\mathcal{R}_0 > 1$, namely 1.006, indicating an outbreak potential, as seen from the increase in infected and quarantined subpopulations and the decrease in susceptible subpopulations. The simulation in Figure 10 shows that the final number of infected subpopulation (I) when $\beta = 0.09$ is 0.0081 (Figure 10d), while this number increases to 0.0087 when $\beta = 0.9$. Similarly, Figure 10f shows the quarantined subpopulation (Q) increases from 0.0635 to 0.0695, and Figure 10g shows the recovered subpopulation (R) increases from 2.2902 to 2.3744.

Meanwhile, Figure 10a illustrates the variation of β against the highly susceptible, unvaccinated subpopulation S_1, showing a decline from 25.0077 to 24.9736 as β increases from 0.09 to 0.9. Concurrently, Figure 10b depicts the variation of β against the vaccinated susceptible subpopulation S_2, which decreases from 1.7262 to 1.7071 over the same parameter range. This shows that a higher transmission rate accelerates the transition from the susceptible subpopulation to the exposed, infected, and finally recovered subpopulations. Thus, the relationship between β and the spread of diphtheria is positive, meaning that when the value of β increases, diphtheria outbreaks also spread. However, in the variation of β, the number of infected subpopulations is not too large, because there are other factors that influence this, namely quarantine and vaccination.

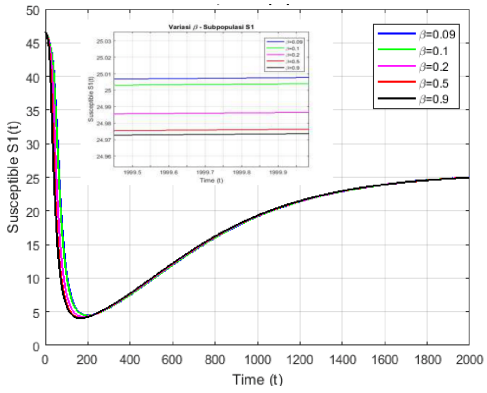

(a) Variation of β against S_1

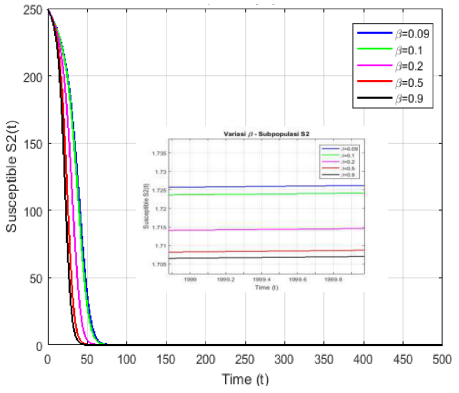

(b) Variation of β against S_2

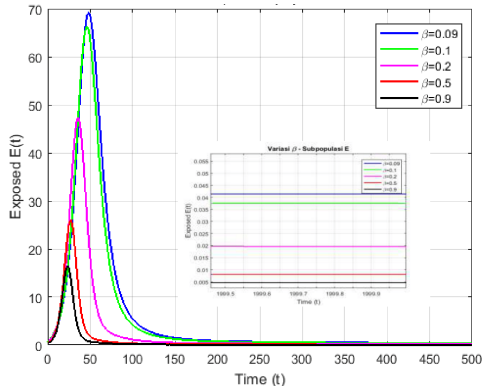

(c) Variation of β against E

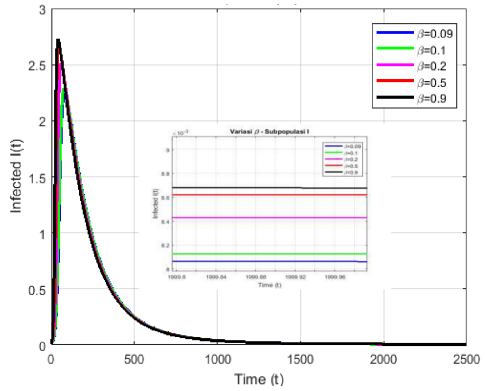

(d) Variation of β against I

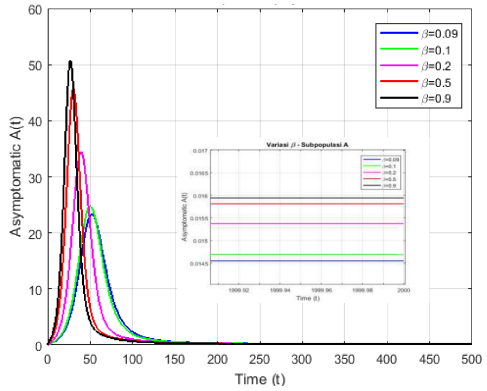

(e) Variation of β against A

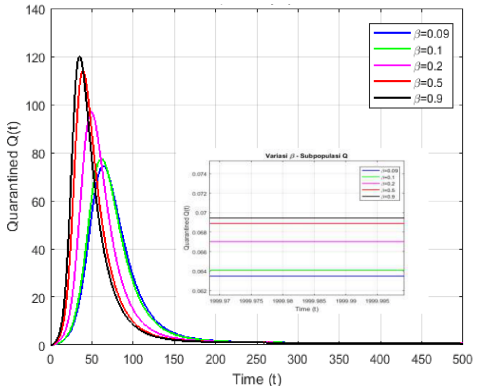

(f) Variation of β against Q

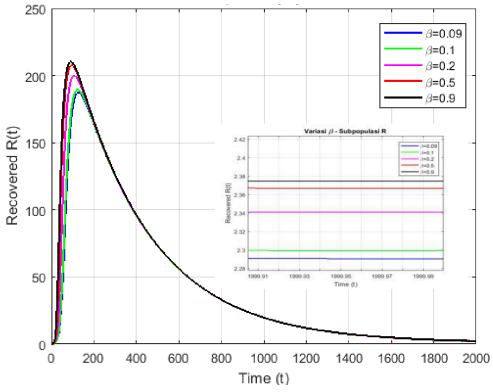

(g) Variation of β against R

Figure 10: Numerical solution of model (2.1) parameter variation β

4. Conclusions

We present a comprehensive study of a fractional-order diphtheria model that incorporates two critical features: susceptibility heterogeneity and an asymptomatic infected population, S_1S_2EIAQR. The mathematical analysis of boundedness, positivity, and existence and uniqueness are studied. Based on the dominant eigenvalue FV^{-1}, the basic reproduction number ($\mathcal{R}_0$) can be obtained, where this basic reproduction number provides information about the transmission of a disease in a closed population. If $\mathcal{R}_0 < 1$, the disease gradually disappears, it indicates a disease-free state. Conversely, if $\mathcal{R}_0 > 1$, the disease spreads further, indicating an endemic state. The local stability for disease-free equilibrium point is proved by applying the Matignon's Condition. The global asymptotic stability of the disease-free equilibrium is examined by applying the approach proposed by 10. The global stability of the endemic equilibrium point is established by constructing the appropriate Lyapunov function. Next, the predictor-corrector technique is used for the numerical simulation approach. This numerical simulation is intended to obtain results of the fractional order effects on the model. By simulating different α values, namely: $\alpha = 0.8$, $\alpha = 0.85$, $\alpha = 0.87$, $\alpha = 0.9$, $\alpha = 0.95$, $\alpha = 0.97$, and $\alpha = 1$, the α value $\alpha = 0.8$ was obtained which had the smallest RMSE (822.42), so that the model provided better predictions than other α. Finally, we implemented real data to validate the fractional dynamics system by matching the numerical results using the fifth-order and fourth-order Runge-Kutta method with diphtheria case data in Indonesia in 2012–2023. Based on the RMSE value, we can conclude that a smaller fractional order guarantees a smaller RMSE value, that can be used to reduce the diphtheria outbreaks and to improve the vaccination usage.

Decleration

Availability of Data and Materials: Data were obtained from the Ministry of Health of the Republic of Indonesia and are available at the link `https://kemkes.go.id/id/category-download/profil-kesehatan`.

Competing Interest: The authors declare that there is no competing financial interest or personal relationship that could have appeared to influence the work reported in this paper.

Funding: The first author was supported by Beasiswa Indonesia Bangkit - Education Fund Management Institution (LPDP) - Ministry of Religion of the Republic of Indonesia with number REG20250519017.

Author's Contributions: Mohamad Tafrikan: Conceptualization, Modification, Formal analysis, Investigation, Writing—original draft. Fatmawati: Modification, Formal analysis, Writing—Review & Editing. Windarto: Investigation, Supervision. Chinwendu E. Madubueze: Writing—Review & Editing, and Supervision.

Acknowledgements: The author hereby expresses his gratitude to all parties who have contributed to the success of this research, especially to the reviewers who have provided constructive suggestions.

References

[1] S. O. Adewale, S. O. Ajao, I. A. Olopade, G. A. Adeniran, and I. T. Mohammed, "Mathematical analysis of quarantine on the dynamical transmission of diphtheria disease solving Riccati equation using Adomian decomposition method," *International Journal of Scientific and Engineering Investigations* 6 (2017), 8–17. 1

[2] P. Agarwal and R. Singh, "Modelling of transmission dynamics of Nipah virus (NiV): A fractional order approach," *Physica A* 547 (2020), 1–11. 2.3.2

[3] P. Agarwal, S. Deniy, S. Jain, A. A. Alderremy, and S. Aly, "A new analysis of a partial differential equation arising in biology and population genetics via semi-analytical techniques," *Physica A: Statistical Mechanics and its Applications* 542 (2020), 1–27. 1

[4] P. Agarwal, H. Nasrolahpour, N. Maamri, J. C. Trigeassou, R. Nasrolahpour, and S. Momani, "Dynamics of DNA methylation: Fractional model approach," *Progress in Fractional Differentiation and Applications* 11 (2025), 653–660. 1

[5] E. Ahmed, A. M. A. El-Sayed, and H. A. A. El-Saka, "On some Routh–Hurwitz conditions for fractional order differential equations and their applications in Lorenz, Rössler, Chua and Chen systems," *Physics Letters A* 358 (2000), 1–4. 2.3.3

[6] R. Arora, D. Kumar, I. Jhamb, A.K. Narang, "Mathematical modeling of Chikungunya dynamics: Stability and simulation." Cubo (Temuco), 22(2) (2020), 177-201. 1

[7] Anderson, "What to know about diphtheria," [Online]. Available at: `https://www.webmd.com/a-to-z-guides/what-to-know-diphtheria-causes`. Accessed: Jun. 10, 2024. 1

[8] A. Atangana and D. Baleanu, "New fractional derivatives with non-local and non-singular kernel: Theory and application to heat transfer model," *Thermal Science* 20 (2016), 763–769. 1

[9] D. Baleanu, M. Hassan Abadi, A. Jajarmi, K. Zarghami Vahid, and J. J. Nieto, "A new comparative study on the general fractional model of COVID-19 with isolation and quarantine effects," *Alexandria Engineering Journal* 61 (2022), 1119–1131. 1

[10] F. Brauer and C. Castillo-Chavez, "Epidemic models," *Mathematical Models in Population Biology and Epidemiology* (2008), 345–409. 1, 2.3.4

[11] M. Caputo and M. Fabrizio, "A new definition of fractional derivative without singular kernel," *Progress in Fractional Differentiation and Applications* 1 (2015), 73–85. 1

[12] Centers for Disease Control and Prevention, "Diphtheria," [Online]. Available at: `https://www.cdc.gov/diphtheria/about/causes-transmission.html`. 1

[13] S. K. Choi, B. Kang, and N. Koo, "Stability for Caputo fractional differential systems," *Abstract and Applied Analysis* 2014 (2014), 631419. 2.2

[14] C. W. Chukwu, Fatmawati, M. I. Utoyo, A. Setiawan, and J. O. Kanni, "Fractional model of HIV transmission on workplace productivity using real data from Indonesia," *Mathematics and Computers in Simulation* 225 (2024), 1–15. 1

[15] P. N. Das, "Comparative analysis of fractional-order and classical ODE models in explaining real-world dynamics," *Applied Mathematics and Biosystems* 1 (2025), 25–31. 1

[16] V. den Driessche and J. Watmough, "Reproduction numbers and sub-threshold endemic equilibria for compartmental models of disease transmission," *Mathematical Biosciences* 180 (2002), 29–48. 2.3.2

[17] K. Diethelm, *The Analysis of Fractional Differential Equations: An Application-Oriented Exposition Using Differential Operators of Caputo Type*, Springer, 2010. 2.1, 2.2

[18] K. Diethelm, N. J. Ford, and A. D. Freed, "A predictor–corrector approach for the numerical solution of fractional differential equations," *Nonlinear Dynamics* 29 (2002), 3–22. 3.1

[19] I. S. Fauzi et al., "Assessing the impact of booster vaccination on diphtheria transmission: Mathematical modeling and risk zone mapping," *Infectious Disease Modelling* 9 (2024), 245–262. 1

[20] M. Ghani, I. Q. Utami, F. W. Triyayuda, M. Afifah, and A. Suryanto, "A fractional SEIQR model on diphtheria disease," *Modeling Earth Systems and Environment* 9 (2023), 1–12. 1, 2.1, 2.3.2

[21] M. Ghani, "Diphtheria transmission prediction by extended Kalman filter," *MethodsX* 103281 (2025). 3.1

[22] G. T. Haile, P. R. Koya, and F. M. Legesse, "Sensitivity analysis of a mathematical model for malaria transmission accounting for infected ignorant humans and relapse dynamics," *Frontiers in Applied Mathematics and Statistics* 10 (2025), 1–15. 3.2, 3.1

[23] H. Hethcote, "Three basic epidemiological models," *Applied Mathematical Ecology* (1989), 119–144. 1

[24] J. Huo, H. Zhao, and L. Zhu, "The effect of vaccines on backward bifurcation in a fractional order HIV model," *Nonlinear Analysis: Real World Applications* 26 (2015), 289–305. 2.7

[25] F. Ilahi and A. Widiana, "The effectiveness of vaccine in the outbreak of diphtheria: Mathematical model and simulation," *IOP Conference Series: Materials Science and Engineering* 434 (2018), 012006. 1

[26] Z. Islam, S. Ahmed, M. M. Rahman, M. F. Karim, and M. R. Amin, "Global stability analysis and parameter estimation for a diphtheria model: A case study of an epidemic in Rohingya refugee camp in Bangladesh," *Hindawi* 2022 (2022), 1–13. 1

[27] N. Izzati, A. Andriani, and R. Robi'aqolbi, "Optimal control of diphtheria epidemic model with prevention and treatment," *Journal of Physics: Conference Series* 1663 (2020), 012042. 1

[28] R. Kaur, Prabhanshi, I. Jhamb, and P. Verma, "Transmission dynamics of COVID-19 across a region: A mathematical model," *A Phys. Sci.* 95 (2025), 295–310. 1

[29] W. Kermack and A. McKendrick, "A contribution to the mathematical theory of epidemics," *Proceedings of the Royal Society of London* 115 (1927), 700–721. 1

[30] S. R. Lamichhane, "Diphtheria," *StatPearls*, [Online]. Available at: `https://www.ncbi.nlm.nih.gov/books/NBK560911/`. Accessed: Sep. 15, 2024. 1

[31] H. L. Li, L. Zhang, C. Hu, Y. L. Jiang, and Z. Teng, "Dynamical analysis of a fractional-order predator-prey model incorporating a prey refuge," *Journal of Applied Mathematics and Computing* 54 (2017), 435–449. 2.3, 2.2, 2.2

[32] Y. Li, Y. Q. Chen, and I. Podlubny, "Stability of fractional-order nonlinear dynamic systems: Lyapunov direct method and generalized Mittag-Leffler stability," *Computers and Mathematics with Applications* 59 (2010), 1810–1821. 2.3, 2.2, 2.2

[33] C. E. Madubueze, K. A. Tijani, and Fatmawati, "A deterministic mathematical model for optimal control of diphtheria disease with booster vaccination," *Healthcare Analytics* 4 (2023), 100281. 1

[34] D. Matignon, "Stability results on fractional differential equations to control processing," in *Proceedings of the 1996 IMACS Multiconference on Computational Engineering in Systems and Application Multiconference*, Lille, France, vol. 2 (1996), 963–968. 2.3.3

[35] Ministry of Health of the Republic of Indonesia, *Guidelines for Prevention and Control of Diphtheria*, [Online]. Available at: `https://sehatnegeriku.kemkes.go.id/wp-content/uploads/2018/01/buku-pedoman-pencegahan-dan-penanggulangan-difteri.pdf`. Accessed: Jun. 11, 2024. 1

[36] Ministry of Health of the Republic of Indonesia, *Indonesian Health Profile 2023*, [Online]. Available at: `https://kemkes.go.id/id/category-download/profil-kesehatan`. Accessed: Jun. 12, 2024. 1, 3.1

[37] R. R. Musafir, A. Suryanto, I. Darti, and Trisilowati, "Dynamics and optimal control of fractional-order monkeypox epidemic model with social distancing habits and public awareness," *Computer Methods and Programs in Biomedicine Update* 7 (2025), 100187. 1

[38] National Health Service, "Diphtheria," [Online]. Available at: `https://www.nhs.uk/conditions/diphtheria/`. Accessed: Jun. 10, 2024. 1

[39] K. W. D. Nugraha, Setiaji, F. Sibuea, and B. Hardhana, *Profil Kesehatan Indonesia*, Kementerian Kesehatan Republik Indonesia, Jakarta, 2021. 3.1

[40] Z. M. Odibat and N. T. Shawagfeh, "Generalized Taylor's formula," *Computers and Mathematics with Applications* 186 (2007), 286–293. 2.4, 2.5

[41] O. J. Peter, N. D. Fahrani, Fatmawati, Windarto, and C. W. Chukwu, "A fractional derivative modeling study for measles infection with double dose vaccination," *Healthcare Analytics* 4 (2023), 100231. 1

[42] S. Peddinti and Y. Sabbani, "Mathematical modeling of infectious disease spread using differential equations and epidemiological insights," *Frontiers in Applied Mathematics and Statistics* 15 (2024), 114–122. 1

[43] I. Petras, *Fractional-Order Nonlinear Systems: Modeling, Analysis and Simulation*, Higher Education Press, Beijing, 2011. 2.3.3

[44] S. G. Puspita and M. Kharis, "Pemodelan matematika pada penyebaran penyakit difteri dengan pengaruh karantina dan vaksinasi," *Unnes Journal of Mathematics* 6 (2017), 26–34. 1

[45] N. Rahmi and M. I. Pratama, "Model analysis of diphtheria disease transmission with vaccination, quarantine, and handwashing behavior," *JTAM: Jurnal Teori dan Aplikasi Matematika* 7 (2023), 462–473. 1

[46] K. Rodgers, "Diphtheria," *Encyclopaedia Britannica*, [Online]. Available at: `https://www.britannica.com/science/diphtheria`. Accessed: Jul. 10, 2024. 1

[47] W. Saleh and A. Kilieman, "Note on the fractional Mittag-Leffler functions by applying the modified Riemann–Liouville derivatives," *Boletim da Sociedade Paranaense de Matemática* 37 (2019), 45–52. 2.1

[48] A. Shakeel, S. Ullah, and R. Faiza tul, "Numerical computations of fractional differential equations in engineering using the polynomial least squares method," *Journal of Prime Research in Mathematics* 2 (2025), 13–24. 1

[49] M. Shams, N. Kausar, P. Agarwal, S. Jain, M. A. Salman, and M. A. Shah, "On family of the Caputo-type fractional numerical scheme for solving polynomial equations," *Taylor & Francis* 31 (2023), 1–21. 1

[50] M. Sholeh, "Stability analysis of the SIQR model of diphtheria disease spread and migration impact," *Barekeng: Journal of Mathematics and Its Applications* 19 (2025), 173–184. 1

[51] R. Singh, A. U. Rehman, M. Masud, H. A. Alhumzani, S. Mahajan, A. K. Pandit, and P. Agarwal, "Fractional order modeling and analysis of dynamics of stem cell differentiation in complex network," *AIMS Mathematics* 7 (2022), 5175–5198. 1

[52] K. Sornbundit, W. Triampo, and C. Modchang, "Mathematical modeling of diphtheria transmission in Thailand," *Computers in Biology and Medicine* 87 (2017), 162–168. 1

[53] M. Torrea, J. L. Torrea, and D. Ortega, "A modeling of a diphtheria epidemic in the refugee camps," *bioRxiv* (2017), 208835. 1

[54] Trisilowati, I. Darti, R. R. Musafir, M. Rayungsari, and A. Suryanto, "Dynamics of a fractional-order COVID-19 epidemic model with quarantine and standard incidence rate," *Computer Methods and Programs in Biomedicine Update* 7 (2025), 100176. 1

[55] C. Vargas-De-Leon, "Volterra-type Lyapunov function for fractional-order epidemic systems," *Communications in Nonlinear Science and Numerical Simulation* 24 (2015), 75–85. 2.6

[56] WHO, "Diphtheria," [Online]. Available at: `https://www.who.int/news-room/questions-and-answers/item/diphtheria`. Accessed: Jun. 10, 2024. 1

[57] T. Witelski and M. Bowen, *Methods of Mathematical Modelling: Continuous Systems and Differential Equations*, Contin. Syst. Differ. Equations (2015), 23–45. 1